International Journal of Multiphase Flow 165 (2023) 104473

Contents lists available at ScienceDirect

International Journal of Multiphase Flow

journal homepage: www.elsevier.com/locate/ijmulflow

Slug flows of gas and shear-thinning fluids in horizontal pipes

R. Baungartner [b], G.F.N. Gonçalves [b], J.B.R. Loureiro [a,b,*], A.P. Silva Freire [a,b]

[a] Interdisciplinary Center for Fluid Dynamics (NIDF/UFRJ), R. Moniz Aragão 360, 21941-594, Rio de Janeiro, Brazil
[b] Mechanical Engineering Program (PEM/COPPE/UFRJ), C.P. 68503, 21941-972, Rio de Janeiro, Brazil

ARTICLE INFO

Keywords:
Slug flow
Shear-thinning
Non-Newtonian
Unit cell model

ABSTRACT

Experiments on slug flow are carried out with air and three solutions of carboxymethylcellulose (CMC)(0.05, 0.1 and 0.2% w/w) in a 44.2 mm ID horizontal pipe. The lengths, velocities and frequency of passage of the large bubbles are obtained through a high-speed digital camera. The gas fraction and length of liquid slugs are also estimated. Pressure changes along the pipe are measured with a differential pressure transducer. Particle Image Velocimetry is used to obtain the mean velocity of the continuous liquid field in the film and slug regions. The combination of tested gas and liquid superficial velocities and of distinct fluid rheology results in 48 different experimental conditions. The flow behavior is found to be strongly dependent on the rheological properties of the continuous phase. In particular, the gas volume fraction within the liquid slug ($\alpha = 1 - R_s$), the passage frequency of the large bubbles (ν_t) and the pressure changes are increased. New expressions are proposed for α and ν_t to account for the rheology of the liquid phase. Predictions of the flow parameters obtained through two modified mechanistic models are compared with the experimental data. The friction coefficient expression proposed by Anbarlooei et al. (Phys. Rev. E, 92(6), 5–9, 2015) is also tested. The impact of the proposed modifications on the calculated properties of slug flow is assessed; typical RMS-errors of less than 15% are obtained for parameter predictions.

1. Introduction

Drilling fluids must posses the ability to lubricate drill bits and successfully transport debris out of a well bore. The carrying capacity of a fluid flow depends on various parameters, including the geometry of the system, the cuttings features, the physical properties of the fluid and the dynamical properties of the flow.

Normally, the drilling fluid is pumped down through the drill string (a region of high shear rates) and up between the gap defined by the drill string and the formation being drilled (a region of low shear rates). This configuration makes shear-thinning fluids very effective drilling fluids since they exhibit low viscosity at high shear rates and high viscosity at low shear rates. The low viscosity in the drill string reduces the energy losses due to friction whereas the high viscosity in the annular region is efficient for hole cleaning.

Depending on the conditions in which the well is to be drilled, the hydrostatic pressure of the drilling fluid must be controlled as compared to the pore pressure of the sedimentary formation. Operations where the pore pressure exceeds the hydrostatic pressure of the drilling fluid are called underbalanced drilling (UBD). To achieve UBD conditions, the general practice is to inject gas in the drilling fluid. An obvious impact on operations is the resulting more complicate estimation of the control parameters – in particular, local pressure – in a complex two-phase flow.

The purpose of the present work is to study the hydrodynamic properties of air/shear-thinning liquid slug flows in horizontal pipes. Shear-thinning fluids can be described by a two-parameter power-law rheological model. Experiments are introduced to investigate the global and local properties of flows of different carboxymethylcellulose (CMC) solutions. Three solutions are tested with CMC concentrations of 0.05, 0.1 and 0.2% w/w. The resulting rheological behavior of the mixtures is close to that of a power-law fluid with indexes $n = 0.715$, 0.642 and 0.619 respectively. To each non-Newtonian fluid, the superficial velocities of the gas and liquid phases are varied three times. Thus, twelve different experimental conditions are defined for each given fluid rheology (including also the condition $V_{SG} = 0$). In addition to pressure and flow rate measurements, the lengths, velocities and frequency of passage of the large bubbles are determined. The gas fraction and length of liquid slugs are also obtained. Particle Image Velocimetry is used to obtain the mean velocity and turbulent kinetic energy of the continuous liquid field in the film and slug regions.

The experimental data is subsequently used to propose working relations to be used in unit cell models for the description of slug

* Corresponding author at: Interdisciplinary Center for Fluid Dynamics (NIDF/UFRJ), R. Moniz Aragão 360, 21941-594, Rio de Janeiro, Brazil.
E-mail address: jbrloureiro@mecanica.coppe.ufrj.br (J.B.R. Loureiro).

https://doi.org/10.1016/j.ijmultiphaseflow.2023.104473
Received 6 February 2022; Received in revised form 20 January 2023; Accepted 5 April 2023
Available online 11 April 2023

flows. The flow features are found to be strongly influenced by the rheological behavior of the fluid. In particular, new expressions are proposed for the frequency of passage of unit cells (ν_t) and the liquid volume fraction within the liquid slug (R_s). The new correlations are implemented in the unit-cell approaches of Dukler and Hubbard (1975) and Orell (2005) to provide predictions on pressure loss and other flow parameters. The friction-coefficient formulation of Anbarlooei et al. (2015b,a) for power-law fluids is incorporated to the two theories for the prediction of energy loss in the liquid slug. All model predictions are compared with the experimental data. Typically, a RMS error of 15% was obtained.

The following section briefly introduces comments on previous works of slug flow of non-Newtonian fluids. The general configuration of the experiment, the instrumentation and rheological properties of the fluid are presented in Section 3. Section 4 briefly discusses the unit cell models of Dukler and Hubbard (1975) and Orell (2005) for Newtonian flow and the friction coefficient formulation of Anbarlooei et al. (2015a,b) for power-law fluids. The experimental results on slug flow of air and the fluid mixtures of water and CMC are shown in Section 5 (Section 5.1). New correlations for R_s and ν_t are developed in Section 5.2. Predictions furnished by the new correlations applied to the models of Dukler and Hubbard (1975) and Orell (2005) are presented in Section 5.3.

2. Short comments on previous works

According to Xu et al. (2009), Xu (2010) and Picchi et al. (2015) studies on the behavior of slug flow of non-Newtonian fluids are rare in the literature. Possibly, the pioneering work on two-phase flow of non-Newtonian fluids is due to Oliver and Hoon (1968). These authors performed visual studies of flow patterns for various conditions and particularly reported that "in the slug-flow regime, the two-phase pressure drop is sometimes less than that of the liquid flowing alone".

Rosehart et al. (1975) carried out the first detailed study on the characteristics of non-Newtonian slug flow. Capacitive sensors were used to collect data on slug velocity, frequency and average holdup, from which correlations were introduced. Otten and Fayed (1976) followed up with measurements of pressure drop in two-phase flows with solutions of *Carbopol® 941*. Chhabra and Richardson (1984) discussed flow pattern maps for shear-thinning and viscoelastic fluids, observing little difference from the Newtonian case.

Recently, interest has resurfaced on the study of slug flow of non-Newtonian fluids. Xu et al. (2009) have investigated the effect of gas injection in power-law fluid flow on drag reduction. The work basically presents data on flow rates and pressure; predictive models, however, do not fully consider the effects of the liquid rheology. The paper of Jia et al. (2011) discusses fully stratified and slug flows of gas and shear-thinning fluid. To model slug flow, a rearranged set of unit cell equations is introduced. Three dimensional CFD simulations are also presented, and the $\kappa-\epsilon$ model with a low-Reynolds number formulation is used to represent wall turbulence. Effects of flow rheology on the friction coefficient (but for laminar flow), damping parameters and equations of motion are not taken into account.

Picchi et al. (2015) carried out experiments on stratified, plug and slug flows of air and three different carboxymethyl cellulose (CMC) solutions. A high-speed camera was used to identify the flow patterns. The unit cell model of Orell (2005) for slug flow was extended to account for the rheology of the shear-thinning fluid. In particular, the frequency of passage of bubbles was modeled through a modified Gregory and Scott (1969) correlation.

3. Experiments

The present experiments were performed in the Multiphase Flow Laboratory of the Interdisciplinary Centre for Fluid Dynamics (NIDF) of the Federal University of Rio de Janeiro (UFRJ).

3.1. Experimental setup and instrumentation

A general overview of the horizontal multiphase flow loop is given in Fig. 1. The test facility consists of an acrylic pipe with total length of 12 m and internal diameter of 44.2 mm. The fluid mixtures (water and CMC) were prepared and stored in a tank with capacity of 1.0 m^3. A progressing cavity pump was used to transport the liquid phase at a constant flow rate, thus minimizing the occurrence of high shear rates that would otherwise contribute to fluid degradation. An air compressor (Schulz SRS 60) injected dry air (humidity < 1%) into the system through a T-junction located upstream of a 90° bend. The fluid flow rate was controlled through an electromagnetic flow meter (Promag 10P40), with a maximum uncertainty of 0.5%. The gas flow rate was measured with a vortex flow meter (Techmeter FLP04-G2NA) and a maximum uncertainty of 3%. Absolute pressure (Rosemount 800 PSI) and temperature (Siberius KT300) were measured to determine the gas properties at the flow condition. A differential pressure transducer (Endress Hauser Deltabar M) was used to measure the pressure gradient along the pipe through a total of twenty pressure taps. The uncertainty for pressure measurements is 0.1%. All experiments were performed in ambient temperature (of about 23.0 °C). The superficial liquid and gas velocities varied in the respective intervals $[0.72, 1.81]$ ms^{-1} and $[0.2, 0.8]$ ms^{-1}.

The liquid volume fraction in the liquid slug was obtained through an in-house conductance sensor based on the design (geometry and processing circuit) introduced and discussed in Ma et al. (1991) and Wang et al. (1991). The concave electrodes (stainless steel) were installed flush to the internal wall to minimize flow interference, arranged in the vertical position and had dimensions of 22.1 × 10 × 2 mm and arc of 160°. Calibrations were performed in a vertical column at the beginning and end of a given set of measurements to make sure results were consistent to within 1%. Results provided by the conductance sensor were also assessed against results provided from an available ITS tomographic system (Model P2+v7.0). The resistivity sensor was preferred in view of its simplicity and good frequency response. The degree of aeration of the liquid slugs was also observed and monitored from the silhouette projections of bubbles through a high speed camera (described below). The visual observations were important to characterize the general spatial distribution of small bubbles.

Inspection windows were centered 4500 and 9000 mm away from the entrance (Fig. 1), respectively at $L/D = 101.8$ and 203.6. The inspection windows were enclosed by rectangular acrylic boxes filled with tap water to minimize optical distortions. A synchronized counting system was used to evaluate the number of bubbles (for a given period of time) that passed through both measuring stations. Typically a reduction of 7% in the number of bubbles was observed at position $L/D = 203.6$.

The characteristics of the dispersed and continuous phases of the flow were determined through the Shadow Size Technique (SS) and Particle Image Velocimetry (PIV). The present procedure is based on the methodologies described in Magalhaes et al. (2013), Matamoros et al. (2014), Celis et al. (2021) and Rosero et al. (2022).

Bubble characteristics, including length, translational velocity and frequency, were measured with the Shadow Sizer Technique. Images were acquired through two NanoSense MkIII cameras (1280 × 1024 pixels, 2080 fps) fitted with lenses AF D Micro-Nikkor 60 mm $f/2.8$. Two constellation LED systems were used to diffuse the background illumination. The image illumination and lens focus were adjusted to provide a high contrast between the bubble contour and the background. For most measurements, the aperture of the lenses was $f/4$ and the focusing distance 50 mm. Typically, the statistics of bubbles – sizes and velocities – were obtained from 5000 images, acquired at a rate of 100 Hz. For system synchronization and image acquisition, the software Dynamic Studio of Dantec Dynamics Inc. was used (version 4.15.115.0). Image processing was made with the software Wolfram

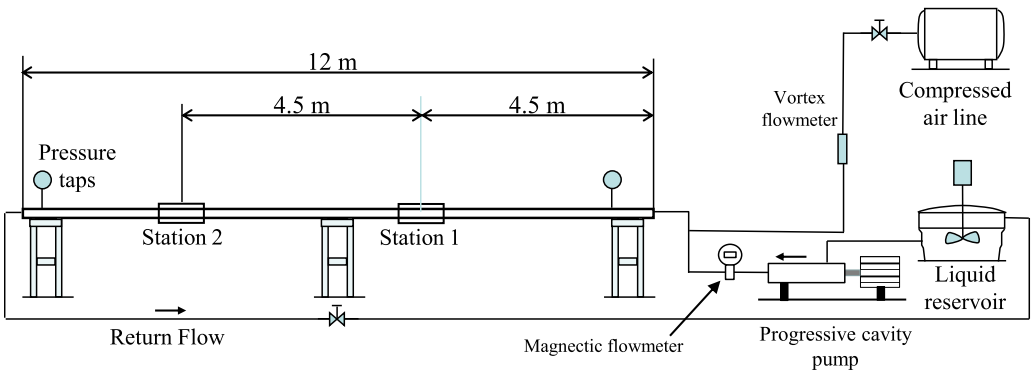

Fig. 1. Schematic diagram of the multiphase flow loop.

Mathematica™. A series of operations including subtraction of the background, brightness and contrast adjustments and image binarization were applied to the images to make the contour of the bubbles sharply defined. Before any two-phase flow data were obtained, 100 images of the single phase liquid flow were captured; the mean of these images was considered the standard for the background gray levels and the relevant dimensions of the flow. The reference length for the 2D calibration was the internal diameter of the pipe. This procedure was repeated any time a new measurement was considered. Bubble reconstruction was made with the tracking method described in Matamoros et al. (2014). Initially, 2000 images were captured at a frequency of 100 Hz. From these data, the bubble velocity was estimated. The procedure was repeated for 20 times to get an average bubble velocity. This velocity was then used to define the acquisition frequency. Two sets of 5000 images were obtained for construction of the statistics, which considered only different bubbles to assure statistical independence of the results.

The PIV system resorted to the same camera, lenses and illumination system used in the SS measurements. A second independent illumination system was used as light source, a double-pulsed Nd:YAG laser that emits at a wavelength of 532 nm. The continuous phase was seeded with Rhodamine particles (1.26 g cm^{-3}). These particles scatter light in the red wavelength, above 570 nm. The constellation LED was covered with a red diffuser, to scatter light on the red wavelength as well. To eliminate reflections of the Nd-YAG laser on the camera lens due to the presence of bubbles and the pipe wall, the camera lens was fitted with a narrow band filter, so that only light scattered from the Rhodamine particles and from the contour of the bubbles could be received at the CMOS sensor. The complete system, including the two sources of light, was synchronized so that the images of the bubbles and the position of the Rhodamine particles are simultaneously captured. The pairs of images were acquired at a frequency of 15 Hz. The time interval between a pair of image varied between 600 to 800 μs depending on the liquid flow rate.

Image processing was used to identify bubble shapes and the position of particles so that the velocity field of the continuous phase and the size and velocity of the bubbles could be simultaneously determined.

Uncertainty calculations were based on the Guide to the Expression of Uncertainty in Measurement (JCGM, 2010). The combined uncertainty was calculated as the square root of the sum of variances estimated from type A (aleatory) and type B (systematic) uncertainties. In the present measurements, aleatory uncertainties were minimized by the acquisition of a large number of samples. The overall or expanded uncertainty was calculated by multiplication of the coverage factor by the combined uncertainty. Considering that the effective degree of freedom is higher than 100, the coverage factor used to express the overall uncertainty with a 90% level of confidence is 1.645. The expanded relative uncertainty for the pressure drop, passage frequency, bubble velocity, liquid slug and bubble lengths, are 0.1%, 0.92%, 1.1%, 5.2%, respectively. Regarding the PIV measurements, the maximum overall uncertainty for the mean velocity measurements is 2%.

3.2. Rheological and physical properties of the working fluids

Carboxymethyl cellulose (CMC) solutions are typically used to simulate the behavior of power-law fluids. Many works show (see, e.g., Benchabane and Bekkour, 2008) that above a critical shear rate, CMC solutions exhibit shear-thinning behavior. In the present investigation, tap water was mixed to CMC (Denvercel FG3000) with concentrations of 0.05, 0.1 and 0.2% w/w. To prevent bacteriological degradation, a mass concentration of 0.03% of formaldehyde was added to the fluid sample. These mixtures provided transparent fluids with low viscoelasticity and high solution stability.

To prepare the CMC solutions, a 50 liter bucket was used to dilute 0.5% w/w solutions that were agitated for about 1.5 h to prevent the formation of polymer agglomerations. These solutions were then subsequently transferred to the main reservoir and further agitated for 1.5 h. Water was added and the homogenization process was repeated until the desired final w/w proportion was achieved, resulting in a very homogeneous solution. To permit the complete hydration of the polymer molecules the resulting mixture was allowed to rest for 24 h. Typically the preparation of the test mixtures lasted for two and a half days. Before running the experiments, the solutions were mixed again for 1.5 h.

The rheological characterization of the CMC-water mixtures was performed in a Thermo Scientific rheometer, model Haake Mars III. A thermostatic bath and temperature control system allowed adjustments of the fluid sample temperature between 4 to 120 °C. The universal measurement unit was fitted with a cone-plate geometry to allow the measurement of viscosity between 5 mPas to 205 mPas at a maximum shear rate of 7500 s^{-1}. Measurements were made under controlled applied stress or shear rate, depending on the ranges of viscosity and shear rate under observation.

At the start and end of each experimental run, a sample of the working fluid was taken so that its rheological properties could be characterized and analyzed to check for fluid degradation. To minimize fluid degradation, the experiments were carried out over periods that typically did not exceed 6 h. This procedure resulted in variations of K and n below 2.5% (Eq. (1)). The typical rheological characteristics of the solutions are presented in Fig. 2.

The resulting fluids showed a behavior that approaches that of a power-law fluid, defined by:

$$\tau = \eta(|\dot{\gamma}|)\dot{\gamma} = K\,|\dot{\gamma}|^{n-1}\,\dot{\gamma}, \tag{1}$$

where the notation is classical and $|.|$ is a Euclidean tensor norm.

The constant K is the proportionality consistency parameter, and n is the flow index, measuring the degree to which the fluid is shear-thickening ($n > 1$), or shear-thinning ($n < 1$).

In view of the large volume of the mixtures considered in the experiments, all the shear-thinning fluids were prepared using tap water. The water underwent two carbon filters to prevent the passage

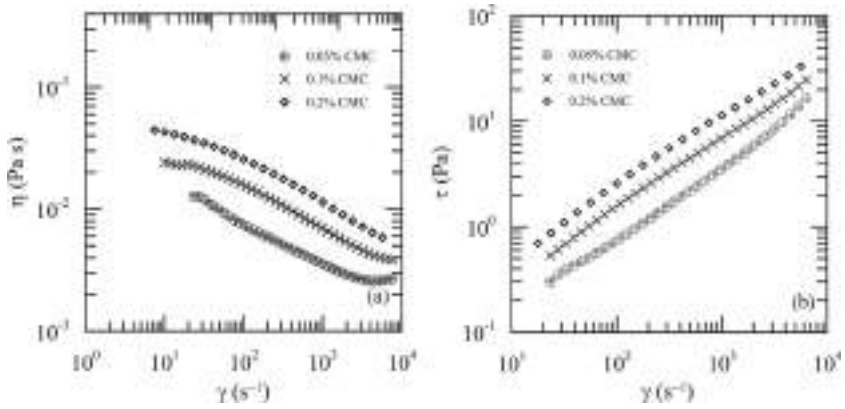

Fig. 2. Characterization of the working fluids: (a) viscometric viscosity and (b) shear stress as a function of the shear rate for the CMC solutions at 23 °C.

Table 1
Rheological properties of the liquids.

Liquid	Concentration c (%w/w)	K (Pa s^n)	n (–)	σ (mN m^{-1})
Water	–	0.0009	1.00	66.69
CMC1	0.05	0.0263	0.715	60.22
CMC2	0.1	0.0827	0.642	57.41
CMC3	0.2	0.1567	0.619	52.47

Table 2
Superficial liquid (V_{SL}) and gas (V_{SG}) velocities for the experiments.

Experiment	V_{SL} [ms^{-1}]	V_{SG} [ms^{-1}]
T1	0.72	0.27
T2	0.72	0.49
T3	0.72	0.78
T4	1.27	0.22
T5	1.27	0.42
T6	1.27	0.68
T7	1.81	0.21
T8	1.81	0.43
T9	1.81	0.65

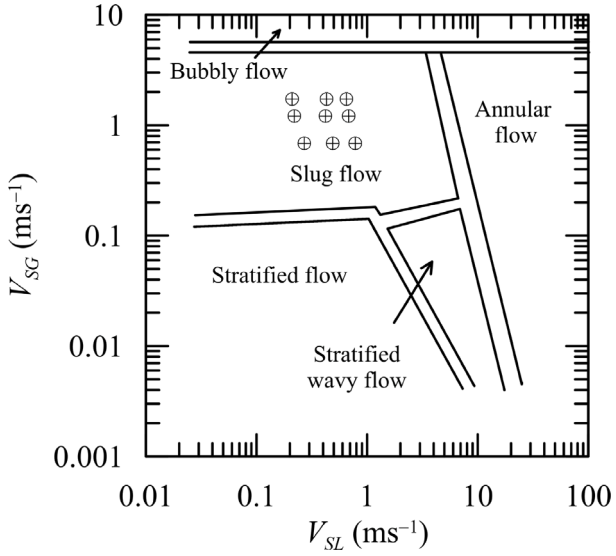

Fig. 3. Experimental conditions according to the flow pattern map for gas/power-law liquid mixtures of Chhabra and Richardson (1984).

of particles above 5 μm. The surface tensions for tap water and every CMC w/w concentration were measured using a K100 tensiometer from Krüss™. The method used by K100 allows the detection of the vertical force by a force sensor when a reference plate makes contact with the liquid surface. The surface tension is evaluated from the measured force and the wet length of the plate. Every surface tension measurement was carried out over 1 h, at 25 °C, to ensure the stabilization of the sample and the measured force by the sensor.

The properties of the fluids are shown in Table 1.

Please, note that Picchi et al. (2015) have reported an increase in surface tension as the CMC concentration increases in a water-CMC mixture. In the present measurements, we have consistently found a reduction in surface tension for the water-CMC mixtures.

3.3. Experimental gas and liquid flow rates

The experimental conditions are shown in the flow pattern map of Chhabra and Richardson (1984) for gas/power-law liquid mixtures (see Fig. 3). Table 2 specifies the adopted superficial gas and liquid velocities.

4. Unit cell models and closure equations

4.1. Unit cell model for slug flow

The inherent complexity of slug flows means that much effort has been dedicated in literature to a proper understanding of its essential mechanisms. In fact, the development of simple and robust methods for the prediction of the mean properties of slug flows is a problem of great importance since most fluid transportation systems exhibit complex geometries with long stretches of pipe and diverse added components. This complexity virtually forbids the sole use of CFD for problem solution. The alternative is to appeal to substantial modeling, strongly supported by correlations derived from experimental data.

The dependence of geometric and dynamic parameters on flow models has been extensively studied in literature, but for most of the available published material the working fluid is Newtonian.

In unit cell models, the chaotic nature of slug flow is encapsulated in a well defined structure that is considered to repeat itself indefinitely. Typically, a unit cell is divided into two regions: the film and liquid slug regions.

In the reference frame that moves with the bubble translational velocity, the flow is treated as a steady flow. The model is based on the balances of mass and momentum and requires empirical correlations for closure. Some of the variables that are usually considered are the frequency of passage of cells (v_t), the liquid volume fraction within the liquid slug (R_s) and the translational velocity (V_t).

In the present analysis, the models of Dukler and Hubbard (1975) and Orell (2005) are considered (Fig. 4). They differ mostly through the choices of closure relations and simplifications. For a full description of

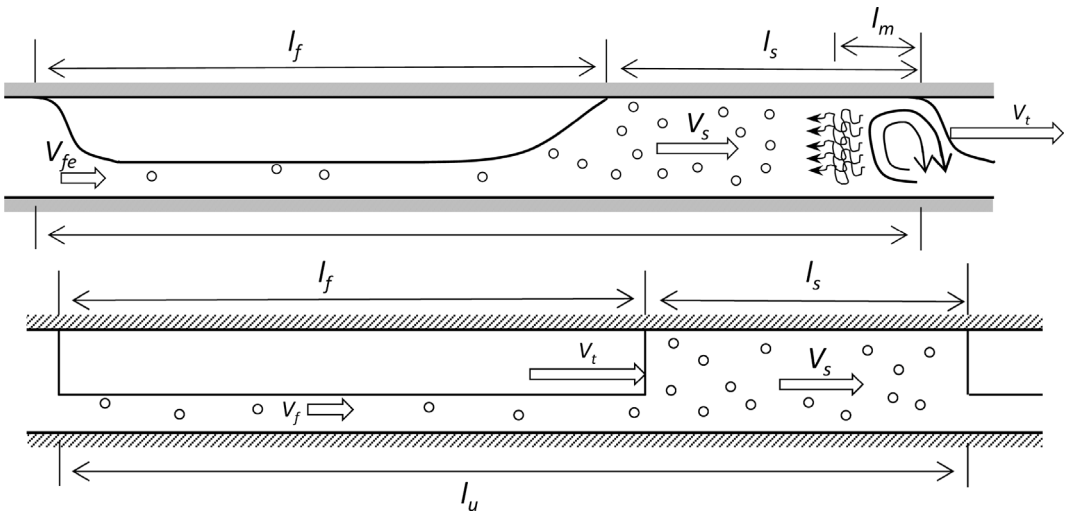

Fig. 4. Unit cell model structures according to the models of Dukler and Hubbard (1975) (top) and Orell (2005) (bottom). l_f = length of the liquid film, l_s = liquid slug length, l_m = mixing vortex region length, V_t = unit cell translational velocity, V_s = liquid slug velocity.

the models, please, refer to the original works, or, alternatively, to Bandeira et al. (2017). The present notation is based on the developments shown in Dukler and Hubbard (1975).

In essence, the slug model of Dukler and Hubbard (1975) consists of a long bubble traveling over a liquid film that is followed by a liquid plug with a strong mixing region at the front (Fig. 4). Since in the film region pressure is essentially constant, pressure losses are confined to the liquid slug region where they can be considered to arise from two effects: the acceleration of the slow moving liquid film to slug velocity and the pressure loss required to overcome the wall shear stress in the main part of the slug. The model of Dukler and Hubbard (1975) needs basically two correlations for closure: v_t and R_s. Here, we use respectively the model of Andreussi et al. (1993) and the correlation of Schulkes (2011).

The model of Orell (2005) is based on the model of Taitel and Barnea (1990), which considers a uniform film thickness (Fig. 4). The model also takes into account the increase of the apparent viscosity in the liquid slug due to the presence of air bubbles. The model of Orell (2005) requires the specification of V_t.

Reviews on further theories for the description of slug flows can be found in Gonçalves et al. (2018) and Fagundes Netto et al. (2019).

4.2. Correlations for v_t

One of the earliest correlations for the prediction of v_t was introduced by Gregory and Scott (1969). In their experiment, gas (CO_2) and liquid (water) were introduced through a tee mixer in a pipe with internal diameter (D) of 3/4" and length of $300D$. An analysis of the experimental data suggested,

$$v_t = 0.0226\left[\frac{V_{SL}}{gD}\left(\frac{19.75}{V_m}+V_m\right)\right]^{1.2}, \tag{2}$$

where V_m is the mixture velocity ($= V_{SL} + V_{SG}$), V_{SL} is the liquid superficial velocity, D is the pipe diameter and g the gravity acceleration. All quantities in the above equation must be expressed in IS units.

The coefficients of Eq. (2) were adjusted by Rosehart et al. (1975) to their own experiment to account for the rheology of the liquid phase. The result was

$$v_t = P_1 Fr_s^{P_2}, \tag{3}$$

where

$$Fr_s = \frac{V_{SL}}{gD}\left(\frac{36.0}{V_t}+V_t\right), \tag{4}$$

and V_t is the translational velocity of the unity cell, $P_1 = 0.0163$ (water), $P_2 = 1.13$ (water), and $P_1 = 0.048$ (CMC mixtures), $P_2 = 0.98$ (CMC mixtures).

Heywood and Richardson (1979) used the same approach to propose

$$v_t = 0.0364\frac{V_{SL}}{V_m}\left(\frac{2.02}{D}+\frac{V_m^2}{gD}\right)^{1.06}. \tag{5}$$

For low viscosity fluids, the following correlation can be used (Shell Correlation)(*apud* Al-Safran, 2009):

$$v_t = \sqrt{\frac{g}{D}}\left\{Fr_{\min} + A_{\text{Shell}}\left[(Fr_{SL}+Fr_{SG})^{0.1} - 1.17(Fr_{SL})^{0.064}\right]^2\right\}, \tag{6}$$

where

$$Fr_{\min} = 0.048 Fr_{SL}^{0.81}, \tag{7}$$

$$A_{\text{Shell}} = 0.73 Fr_{SL}^{2.34}, \tag{8}$$

and Fr_{SL} and Fr_{SG} are the Froude numbers based on the superficial velocities of the liquid and gas phases.

A correlation for very viscous oils was introduced by Gokcal et al. (2009), with the form

$$v_t = 2.623\frac{1.0}{A_r^{0.612}}\frac{V_{SL}}{D}, \tag{9}$$

where the Archimedes number is defined as

$$A_r = D^{1.5}\frac{\sqrt{\rho_L(\rho_L-\rho_G)g}}{\mu_L}. \tag{10}$$

Schulkes (2011) proposed a correlation based on 1200 experimental points. The expression takes into account the physical properties of the flows as well as the diameter and the inclination (β) of the pipe:

$$v_t = \Psi(R_s)\Phi(Re_{SL})\Theta(\beta, Fr_{SL})\frac{V_m}{D}, \tag{11}$$

where

$$\Psi(R_s) = 0.016(5 - 8R_s + 3R_s^2), \tag{12}$$

$$\Phi(Re_{SL}) = \begin{cases} 12.1 Re_{SL}^{-0.37}, & Re_{SL} < 4000, \\ 1.0, & Re_{SL} \geq 4000, \end{cases} \tag{13}$$

$$\Theta(\beta, Fr_{SL}) = \begin{cases} 1 + \frac{2}{Fr_{SL}}\text{sgn}(\beta)\sqrt{|\beta|}, & |\beta| \leq 0.17, \\ \frac{1.8}{Fr_{SL}}(0.6 + 2\beta - \beta^2), & |\beta| > 0.17, \end{cases} \tag{14}$$

where Re_{SL} ($= V_{SL}D/\nu_L$) and Fr_{SL} ($=V_{SL}/\sqrt{gD\cos\beta}$) are the Reynolds and Froude numbers based on the superficial liquid velocity, V_{SL}.

Based on their own data on shear-thinning fluids, Picchi et al. (2015) extended the model of Gregory and Scott (1969) according to

$$\nu_t = 0.0448\left[\frac{V_{SL}}{gD}\left(\frac{32.2014}{V_m}+V_m\right)\right]^{0.88}\left(\frac{Re_{SL}}{Re_{SW}}\right)^{0.07} n^{-2.85}, \tag{15}$$

where Re_{SL} now is based on the generalized Reynolds number (in terms of V_{SL}) and Re_{SW} is the Reynolds number based on the properties of water,

$$Re_{SL} = \frac{\rho_L V_{SL}^{2-n} D^n}{8^{n-1}K\left(\frac{3n+1}{4n}\right)^n}, \quad Re_{SW} = \frac{\rho_W V_{SL} D}{\mu_W}. \tag{16}$$

Note that for $n = 1$, Re_{SL} in Eq. (16) reduces to Re_{SW}.

4.3. Correlations for the liquid volume fraction, R_s

Measurements of liquid fraction in the liquid slug of air–oil flows with a capacitance sensor by Gregory et al. (1978) resulted in

$$R_s = \frac{1.0}{1.0+\left(\frac{V_m}{8.66}\right)^{1.39}}, \tag{17}$$

where R_s is the liquid volume fraction.

To develop a mechanistic model for prediction of R_s, Barnea and Brauner (1985) consider a point on the dispersed bubble–slug transition boundary. The gas fraction at this point is the maximum gas fraction that the liquid slug can accommodate as a fully dispersed bubble pattern for a given turbulence level, and is determined by the mixture velocity. Considering no-slip flow,

$$R_s = 1 - \frac{V_{SG}^{\text{bub}}}{V_m}, \tag{18}$$

where, to determine V_{SG}^{bub}, a flow pattern map is required.

Andreussi et al. (1993) proposed a semi-mechanistic model for the liquid fraction in the liquid slug that considers bubble coalescence and entrainment. The working expression is

$$R_s = 1 - \frac{V_m/\sqrt{gD} - F_0}{V_m/\sqrt{gD} + 2400B_o^{-3/4}}, \tag{19}$$

where:

$$B_o = \frac{(\rho_L-\rho_G)gD^2}{\sigma}, \quad \sigma = \text{surface tension} \tag{20}$$

$$F_0 = 2.6\left[1-2\left(\frac{D_0}{D}\right)^2\right], \tag{21}$$

with $D_0 = 0.025$ meter.

Abdul-Majeed (2000) introduced a correlation based on 435 measurements from 7 distinct sources. The result is

$$R_s = (1.009 - CV_m)A, \tag{22}$$

$$C = 0.006 + 1.3377\frac{\mu_G}{\mu_L}, \tag{23}$$

$$A = \begin{cases} 1.0, & \beta \le 0, \\ 1.0-\sin(\beta), & \beta > 0. \end{cases} \tag{24}$$

Kora et al. (2011) studied the effects of high viscosity on gas fraction. Based on their experiments,

$$R_s = \begin{cases} 1.012\exp\left(-0.085N_{Fr}N_\mu^{0.2}\right), & 0.15 < N_{Fr}N_\mu^{0.2} < 1.5, \\ 0.9473\exp\left(-0.041N_{Fr}N_\mu^{0.2}\right), & N_{Fr}N_\mu^{0.2} \ge 1.5, \\ 1.0, & N_{Fr}N_\mu^{0.2} \le 0.15, \end{cases} \tag{25}$$

with

$$N_{Fr} = \frac{V_m}{\sqrt{gD}}\sqrt{\frac{\rho_L}{(\rho_L-\rho_G)}}, \tag{26}$$

$$N_\mu = \frac{V_m\mu_L}{gD^2(\rho_L-\rho_G)}. \tag{27}$$

For shear-thinning fluids, Xu (2013) introduced a correlation based on the analysis of 360 data points. The non-Newtonian behavior was achieved through a CMC mixture. The correlation is given by

$$R_s = 1 - \frac{(1-\sin\beta)^{0.05}}{1+3.166\times10^{-5}Re_L^{1.225}}, \tag{28}$$

with $Re_L = \rho_L DV_m/\mu_{\text{eff}}$, $0° \le \beta \le 75°$ and

$$\mu_{\text{eff}} = 8^{n-1}K'D^{1-n}V_m^{n-1}. \tag{29}$$

In his work, Xu (2013) mentions K' in Eq. (29) to be the consistency index for a power-law fluid. This is in disagreement with the generalized Reynolds number of Dodge and Metzner (1955) where K' is in fact related to the consistency constant of Eq. (1) through

$$K' = K\left(\frac{3n+1}{4n}\right)^n. \tag{30}$$

Al-Safran et al. (2015) analyzed the performance of several correlations through their own data for very viscous oils. The expression that best fitted the experiments was

$$R_s = 0.85 - 0.075\phi + 0.057\sqrt{\phi^2+2.27}, \tag{31}$$

with

$$\phi = \left(N_{Fr}N_\mu^{0.2} - 0.89\right), \tag{32}$$

and N_{Fr} and N_μ are defined as in Eq. (25).

4.4. Models for V_t

The translational velocity of horizontal large bubbles is normally expressed in the form introduced by Nicklin et al. (1962):

$$V_t = C_0V_m + C_1\sqrt{gD}. \tag{33}$$

Experiments carried out by Bendiksen (1984) with air and water in different pipe slopes suggest

$$C_0 = \begin{cases} 1.05, & Fr_{SL} < 3.5, \\ 1.2, & Fr_{SL} \ge 3.5, \end{cases} \tag{34}$$

$$C_1 = \begin{cases} 0.54, & Fr_{SL} < 3.5, \\ 0, & Fr_{SL} \ge 3.5. \end{cases} \tag{35}$$

Petalas and Aziz (1998) proposed an expression that takes into account some of the physical properties of the fluids. For horizontal flows, the result is

$$C_0 = \frac{1.64}{Re_{mL}^{0.031}}, \quad Re_{mL} = \frac{V_mD}{\nu_L}, \tag{36}$$

$$C_1 = 0.54 - \frac{1.76}{Bo^{0.56}}. \tag{37}$$

Smith et al. (2013) modeled the flow of viscous oils through the correlations

$$C_0 = \frac{(n_f+1)(2n_f+1)}{2n_f^2}, \tag{38}$$

$$C_1 = 0.53\exp(-13.7A_r^{-0.46}B_o^{-0.1}), \tag{39}$$

where:

$$n_f = \frac{1}{\sqrt{f_s}}, \tag{40}$$

and f_s is the friction coefficient of the liquid slug.

4.5. Friction factor for shear-thinning fluids

The flow of purely viscous non-Newtonian fluids received a classical treatment by Metzner and Reed (1955) and Dodge and Metzner (1955). In particular, these references introduced a generalization of the Reynolds number for power-law fluids and a law of resistance for pipe flow.

The derivation of the law of resistance by these authors was based on some asymptotic arguments and on a direct fit of the experimental data to the logarithmic introduced expression. Subsequent works have proposed improvements to the original expression; in particular, Loureiro and Silva Freire (2013) analyzed the data of several authors to determine the functional dependence of the log-law linear coefficients on the power-law index, n. The conclusion was that the angular coefficient of the log-law was constant whereas the linear coefficient varied with the reciprocal of n.

Using arguments based on Kolmogorov's phenomenology theory and their own DNS data, Anbarlooei et al. (2015a,b) proposed an expression for the friction coefficient where the relevant parameters depend on the flow index n. The equation is similar to the Blasius formula and reduces to the Newtonian case in the limit as $n \to 1$. Thus, the equation is explicit and easy to use.

The equation proposed by Anbarlooei et al. (2015a,b), can be cast as

$$f_L = (0.102 - 0.033n + 0.01n^{-1}) Re_{\mathrm{MR}}^{-1/(2(n+1))}, \tag{41}$$

where the generalized Reynolds number of Metzner and Reed (1955) for single phase flows is given by

$$Re_{\mathrm{MR}} = \frac{8\rho D^n V^{2-n}}{K\left(6+\frac{2}{n}\right)^n}, \tag{42}$$

where D denotes the pipe diameter, V is the mean liquid velocity, K is the consistency index and n is the exponent of the power-law model equation.

From Eq. (42) an effective viscosity can be obtained as:

$$\mu_{\mathrm{eff}} = \frac{K\left(6+\frac{2}{n}\right)^n D^{1-n} V^{n-1}}{8\rho}. \tag{43}$$

Some previous works (Xu et al., 2009; Jia et al., 2011; Picchi et al., 2015) on the slug flow of non-Newtonian fluids have adopted the following expression:

$$f_L = C_L Re_{\mathrm{MR}}^{-m}, \tag{44}$$

where, according to Orell (2005), $C_L = 16$ and $m = 1$ for laminar flow, $C_L = 0.046$ and $m = 0.2$ for turbulent flow, and Re_{MR} needs to be specialized for two-phase flows. Normally this specialization is achieved by replacing V and ρ in Eq. (42) by V_m and ρ_m. V_m is the mixture velocity ($= V_{SL} + V_{SG}$) and ρ_m is the mean density of the liquid slug ($= \rho_L R_s + \rho_G(1 - R_s)$).

Very clearly, Eq. (44) cannot correctly represent the effects of the fluid rheology.

Eq. (41) can be extended to Bingham fluids. The analysis, however, is more elaborate and must consider inclusion of the Hedstrom number (see Anbarlooei et al. (2017b)). The arguments first introduced in Anbarlooei et al. (2015a, 2017b) are further generalized in Anbarlooei et al. (2017a) to derive the Kolmogorov micro-scales for general viscoplastic fluid flows. The analysis then relates the Kolmogorov micro-scale velocities to the proposed friction formula.

Here, we incorporate the effects of the fluid rheology on f_L through the expression originally developed in Anbarlooei et al. (2015b) with V_m and ρ_m considered. Eq. (41) is valid for flow of shear-thinning power-law fluids. In fact, the basis to its derivation is the DNS of flows of fluids with n ranging from 0.5 to 1.2 so that shear-thickening power-law fluids are also discussed. The analysis of Anbarlooei et al. (2017a) further considers cases for which n ranges from 0.5 to 2.

In the following, a comparison on the use of Eqs. (44) and (41) for the representation of liquid friction factor in the film and slug regions is carried out.

5. Results

The present section is divided into three parts. The experimental data are initially introduced, followed by their critical analysis and the introduction of new working relations for R_s and v_t. Then, predictions provided by the new correlations are compared with predictions yielded by the correlations of previous works.

5.1. Experiments

5.1.1. Slug flow characteristics

The addition of polymers to water even in very small concentrations leads to marked changes in the fluid rheology (Fig. 2, Table 1) and hence in the flow behavior. In the present experiments, an important aspect of the flow structure was a high degree of aeration of the continuous phase. Since the gas was injected through a "T" connection upstream of the 90°-bend that gives access to the test section (Fig. 1), the resulting increase in flow agitation at the bend provoked considerable bubble breakup, with the consequent appearance of many small dispersed bubbles in the liquid slug.

For the water flow, the bubbles in the liquid slug were observed to be fewer and concentrated in the upper part of the pipe as compared to the CMC-solutions (Figs. 5, 6, 7, 8). With the increase in the concentration of CMC, the viscosity effects were enhanced so that many small bubbles remained dispersed in the continuous phase (film and slug regions). Indeed, the gas fraction in the liquid slug was observed to increase with the increase in the concentration of CMC and to remain reasonably homogeneous throughout the length of the test section.

The enhanced fluid viscosity also had an important effect on the shape of the bubble nose and the instabilities shown in the bubble interface. Comparisons between the air–water flows (Fig. 5) and air-CMC solution flows (Figs. 6, 7, 8) show a significant reduction in surface distortions for the CMC cases, even for the highest liquid and gas superficial velocities.

5.1.2. Evolution of bubble trains

Two high speed cameras were used to evaluate the properties (number, velocities, lengths) of given trains of bubbles at positions 4500 (Station 1) and 9000 (Station 2) mm downstream of the inlet section. The simultaneous recording of the same set of traveling bubbles through Stations 1 and 2 permitted the estimation of the degree of development of the flow. Fig. 9 shows the average number of registered bubbles at both positions for five experimental conditions of air–water flows.

In general, at Station 2 the number of observed bubbles was reduced by 4 to 11% as compared to Station 1 (average value = 7.1%, standard deviation = 3.6%; of all recorded bubbles).

Ujang et al. (2006) have shown that for many experimental conditions, at distances 75-80D downstream of the gas injection point, air–water horizontal slug flows reach a reasonable degree of fully development.

The distributions of the lengths and velocities of the large bubbles are shown in Figs. 10 and 11 for the present experimental conditions T1 to T5. The reduction in the number of bubbles between the two measuring positions results, of course, from the coalescence of large bubbles, provoked by the existence of liquid slugs that are shorter than a minimum stable length. The small number of coalescing bubbles means that the distributions of long bubble lengths vary little from one position to the other.

Fig. 10 shows that the distributions of l_f are almost identical for four of the conditions, and very close for the fifth. The bubble velocity distributions are also very similar (Fig. 11) at both positions for all experimental conditions and are consistent with Eq. (33) (mean V_t). The implication is that the slug properties change relatively little from Station 1 to Station 2, characterizing near stable conditions.

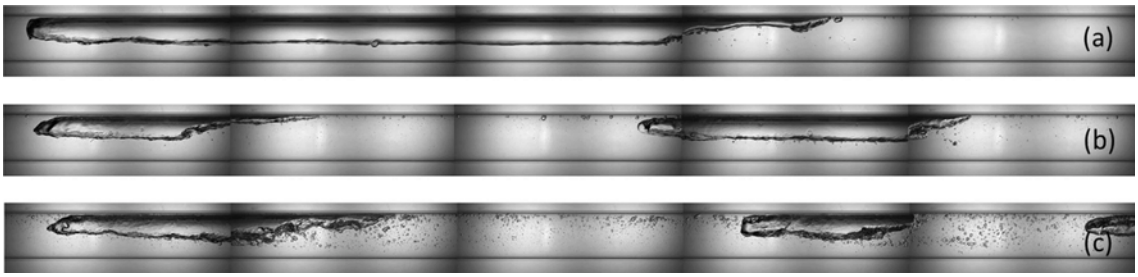

Fig. 5. Air-water slug flow patterns for: (a) $V_{SL} = 0.72$ ms^{-1} and $V_{SG} = 0.27$ ms^{-1}, (b) $V_{SL} = 1.27$ ms^{-1} and $V_{SG} = 0.22$ ms^{-1}, (c) $V_{SL} = 1.81$ ms^{-1} and $V_{SG} = 0.43$ ms^{-1}.

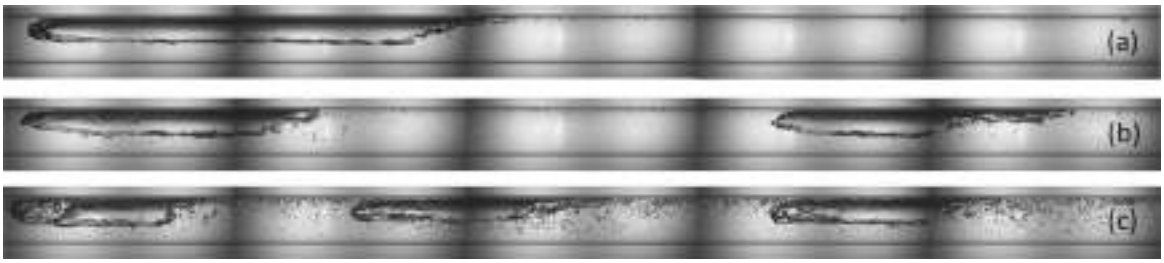

Fig. 6. Air-0.05% CMC solution slug flow patterns for: (a) $V_{SL} = 0.72$ ms^{-1} and $V_{SG} = 0.27$ ms^{-1}, (b) $V_{SL} = 1.27$ ms^{-1} and $V_{SG} = 0.22$ ms^{-1}, (c) $V_{SL} = 1.81$ ms^{-1} and $V_{SG} = 0.43$ ms^{-1}.

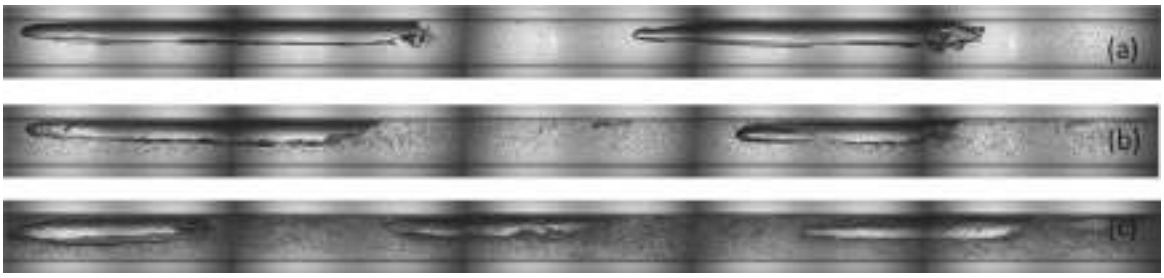

Fig. 7. Air-0.1% CMC solution slug flow patterns for: (a) $V_{SL} = 0.72$ ms^{-1} and $V_{SG} = 0.27$ ms^{-1}, (b) $V_{SL} = 1.27$ ms^{-1} and $V_{SG} = 0.22$ ms^{-1}, (c) $V_{SL} = 1.81$ ms^{-1} and $V_{SG} = 0.43$ ms^{-1}.

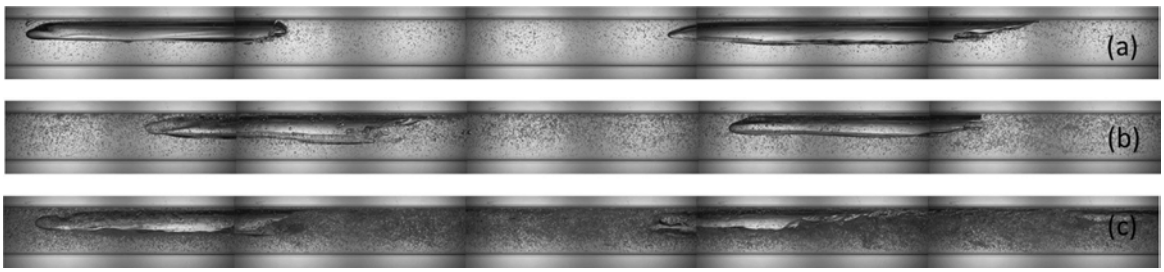

Fig. 8. Air-0.2% CMC solution slug flow patterns for: (a) $V_{SL} = 0.72$ ms^{-1} and $V_{SG} = 0.27$ ms^{-1}, (b) $V_{SL} = 1.27$ ms^{-1} and $V_{SG} = 0.22$ ms^{-1}, (c) $V_{SL} = 1.81$ ms^{-1} and $V_{SG} = 0.43$ ms^{-1}.

5.1.3. Effects of rheology on the total pressure loss

The pressure gradients for all tested conditions are shown in Fig. 12. All flows show a clear increase in the absolute value of dP/dx with decreasing n. In particular, a considerable increase in $|dP/dx|$ can be observed for the highest concentration of CMC (0.2% w/w); for $V_{SL} = 1.27$ ms^{-1} the relative increase is 124%.

5.1.4. Effects of rheology on bubble length

The effects of fluid rheology on the lengths of the long bubbles and the liquid slugs are shown in Figs. 13 and 14. These results are, of course, strongly influenced by the manner in which the gas is injected in the pipe, just upstream of a 90°-bend.

The decrease in n results in shorter bubbles as compared with the Newtonian case. This is particularly apparent for the lowest liquid superficial velocity where reductions in size can be as high as 50%. As V_{SL} increases – and consequently the shear rates – the non-Newtonian viscosity approaches the Newtonian viscosity and so does the length of the large bubbles. For $n = 0.71$, the lengths of the bubbles for $V_{SL} = 1.27$ and 1.81 ms^{-1} are indistinguishable in regard to the fluid rheology. For $n = 0.64$-0.62, the general conclusion is the same: as V_{SL} increases, l_f approaches the Newtonian values, irrespective of the value of n. In relation to the dependence of l_f on V_{SG}, note that as V_{SG} increases, l_f for both cases (Newtonian and non-Newtonian) tend to a same value.

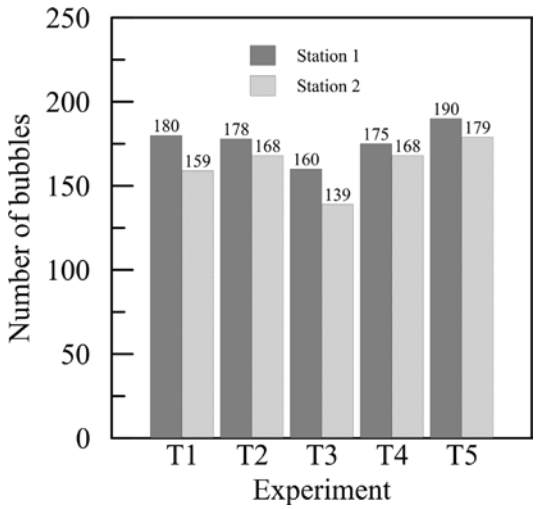

Fig. 9. Number of recorded bubbles at positions Stations 1 and 2 for five experimental conditions of air–water flows.

The dependence of l_s on the rheological properties of the liquid phase and on the superficial velocities is consistent with the previous results for l_f. For water, the lengths of the liquid slugs tend to decrease with the increase in V_{SG} for a fixed V_{SL}. For the non-Newtonian fluids, a considerable reduction in l_s with n is observed only for the condition $V_{SL} = 0.72$. This reduction is of the order of 50%. For all other conditions (changes in n and high V_{SL}), l_s tends to be stable around values about 0.3 m.

The effects of fluid rheology and flow conditions on the size distributions of the long bubbles is shown in Fig. 15. In this figure, n decreases from top to bottom and V_{SL} increases from left to right. One obvious observation is that the mean (m) and the standard deviation (s) values of l_f increase with V_{SG} for all fluid and flow conditions. A secondary conclusion is that m and s decrease with the increase in V_{SL}.

5.1.5. Frequency of passage of long bubbles

Figs. 13 and 14 have shown that, in general, l_f and l_s tend to decrease for non-Newtonian fluids. The immediate consequence would appear to be an increase in the frequency of passage of the long bubbles.

Fig. 16 shows the influence of the flow rate and fluid rheology on the slug frequency. The evidence is that a decrease in n increases the frequency of passage of bubbles (ν_t). This effect is particularly pronounced for the lower liquid flow rates. In fact, for the lowest liquid flow rate, the decrease of n results in an increase in slug frequency of about two times for some conditions ($n \approx 0.64, 0.62$). The gas flow rate exerts little influence on the observed frequencies. As the liquid flow rate increases, the effects of n on ν_t are minimized.

Most of the correlations found in literature for the prediction of ν_t consider V_{SL} and V_m as the dynamic relevant parameters. The physical properties of the flow are not frequently considered since most experiments have been conducted for air and water. The evidence provided by Fig. 16 is that the flow rheology has an important effect on ν_t.

5.1.6. Translational velocity

The translational velocities of the bubbles for different flow rates and power-law indexes are shown in Fig. 17. The shear-thinning behavior induces an increase in the large bubbles translational velocity. A similar trend was observed by Picchi et al. (2015).

The distributions of the translational bubble velocities for conditions T1 and T2 are shown in Fig. 18. The changes in distribution are very small. The rheology of the liquid phase does not affect much the shape of the distributions. The only notable effect is the increase in mean velocity with a decrease in n.

Table 3
Root-mean-square error of R_s ($\sigma^n_{R_s}$) according to the various models and the present experimental data. n denotes Newtonian fluid; nn denotes non-Newtonian fluid.

Reference	$\sigma^n_{R_s}$ (%)	$\sigma^{nn}_{R_s}$ (%)
Abdul-Majeed (2000)	13.4	56.2
Al-Safran et al. (2015)	15.4	49.0
Andreussi et al. (1993)	13.7	50.0
Barnea and Brauner (1985)	17.5	55.3
Gregory et al. (1978)	10.5	41.8
Kora et al. (2011)	15.6	49.3
Xu (2013)	16.4	33.3

5.1.7. PIV results

Before the two-phase flow results are presented, Fig. 19 shows for the sake of comparison the single-phase velocity profiles for $n = 0.71$, 0.64, 0.62 and two mean velocities $V_L = 0.72$ and 1.27 ms^{-1}. As expected, a decrease in n flattens the velocity profile in the central part of the pipe. This is a typical behavior of turbulent shear-thinning fluids, previously reported by Dodge and Metzner (1955) and others. The flow symmetry is also apparent in Fig. 19.

The large number of small bubbles occurring in many of the experimental conditions limited the PIV analysis of the properties of the continuous phase. For this reason, only results obtained with conditions T1 through T4 are reported here.

The general effects of fluid rheology on the velocity fields of the flows around large bubbles are shown in Figs. 20 and 21 for $V_{SL} = 0.72$ ms^{-1}, $V_{SG} = 0.27$ ms^{-1}. The decrease in n provokes a marked increase in the regions of high velocity in the central part of the liquid slug, and in the nose and tail vicinities.

The velocity profiles of the continuous phase in the liquid slugs are shown in Fig. 22 for the four CMC concentrations (0.0-0.05-0.1-0.2% w/w) and flow conditions T1 through T4. The monotonic increase in velocity with the monotonic decrease in n is readily observed. The decrease in n also notably tends to flatten the velocity profiles as previously observed by other authors for single phase flows (Dodge and Metzner, 1955).

The velocity profiles of the continuous phase in the liquid films are shown in Fig. 23 again for the four CMC concentrations (0.0-0.05-0.1-0.2% w/w) and flow conditions T1 through T4. The same trend observed for the slug region is repeated in the film region: a decrease in n provokes an increase in the flow velocity. The increased aeration of the slug and film regions with the decrease of n induces an increase in the flow velocity and the pressure gradient.

5.2. Correlations for R_s and ν_t

5.2.1. R_s behavior for a non-Newtonian liquid phase: analysis of existing correlations and a new formulation

In the present experiments, and for the given entrance conditions, the gas fraction in the liquid slug increases with decreasing n (Fig. 24). The present injection of gas was made upstream of a 90°-bend, meaning that the flow agitation in the bend provoked bubble breakup and resulted in very aerated liquid slugs, in particular, for the CMC-water mixtures.

A comparison between the presently estimated experimental data for R_s and predictions provided by the existing correlations is shown in Table 3. For water, the typical root-mean-square error is 15%. For the non-Newtonian fluids, this value increases to 48%.

To propose a new expression for R_s ($= 1 - \alpha$), the procedures of Barnea and Brauner (1985) and Brauner (2001) are used. The buoyancy acting over a small bubble is given by

$$F_{\text{buoy}} \approx \frac{\pi}{6} d^3 (\rho_L - \rho_G) g, \tag{45}$$

where d is the diameter of the small bubble.

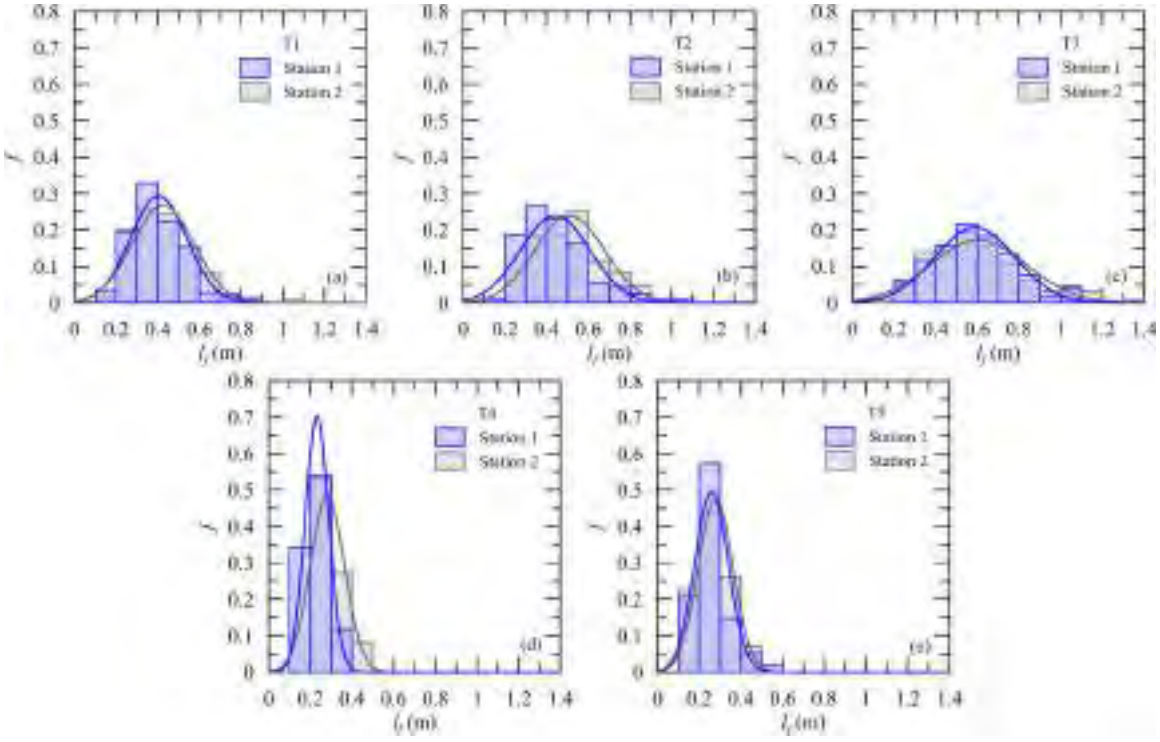

Fig. 10. The distribution of the lengths of large bubbles l_f at positions 4500 mm (Station 1) and 9000 mm (Station 2) for conditions T1 to T5; air-0.1% CMC mixtures. T1: V_{SL} = 0.72 ms^{-1}, V_{SG} = 0.27 ms^{-1}; T2: V_{SL} = 0.72 ms^{-1}, V_{SG} = 0.49 ms^{-1}; T3: V_{SL} = 0.72 ms^{-1}, V_{SG} = 0.78 ms^{-1}; T4: V_{SL} = 1.27 ms^{-1}, V_{SG} = 0.22 ms^{-1}, T5: V_{SL} = 1.27 ms^{-1}, V_{SG} = 0.42 ms^{-1}.

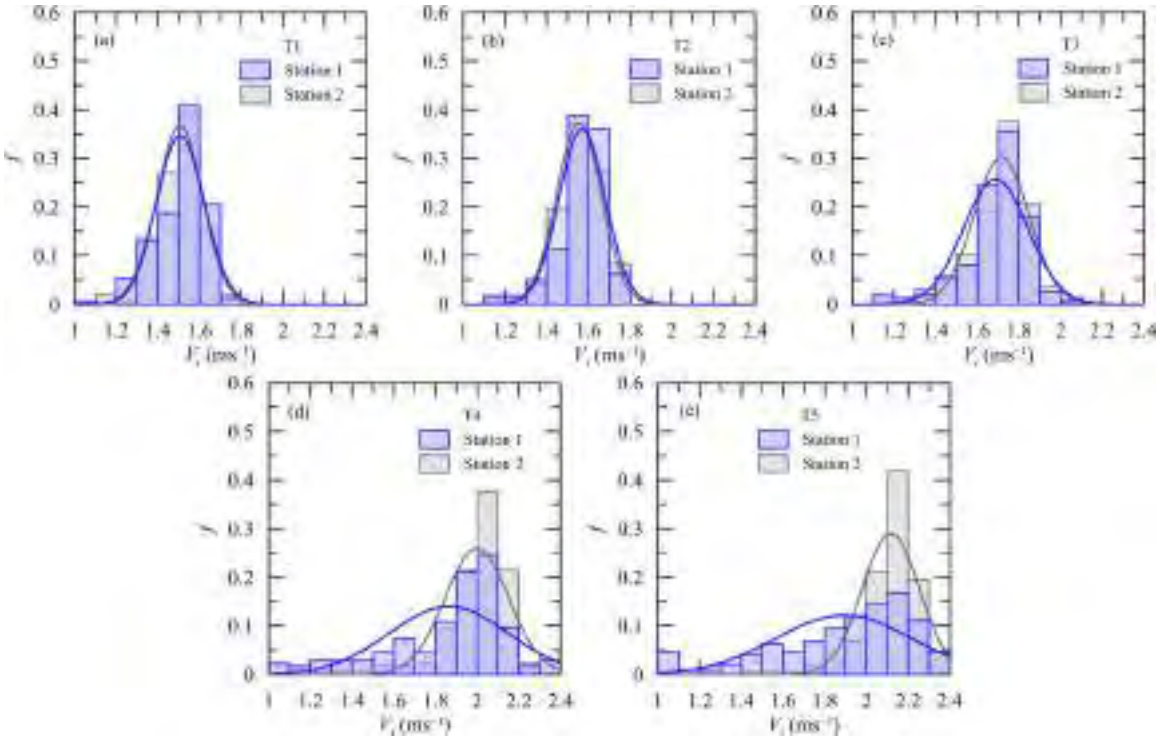

Fig. 11. The distribution of the velocities of large bubbles at positions 4500 mm (Station 1) and 9000 mm (Station 2) for conditions T1 to T5; air-0.1% CMC mixtures. T1: V_{SL} = 0.72 ms^{-1}, V_{SG} = 0.27 ms^{-1}; T2: V_{SL} = 0.72 ms^{-1}, V_{SG} = 0.49 ms^{-1}; T3: V_{SL} = 0.72 ms^{-1}, V_{SG} = 0.78 ms^{-1}; T4: V_{SL} = 1.27 ms^{-1}, V_{SG} = 0.22 ms^{-1}, T5: V_{SL} = 1.27 ms^{-1}, V_{SG} = 0.42 ms^{-1}.

The resistance due to the viscous effects in a power-law fluid is given by

$$F_{\text{visc}} \approx \pi K u^n d^{2-n}, \tag{46}$$

where the characteristic velocity is $u \approx V_m\sqrt{f_L/2}$ (f_L = friction coefficient).

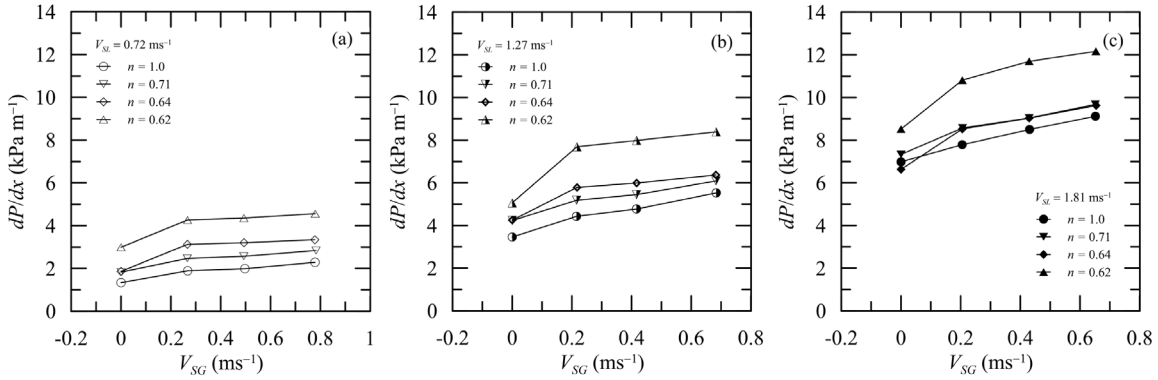

Fig. 12. Total pressure loss for all tested shear-thinning fluids.

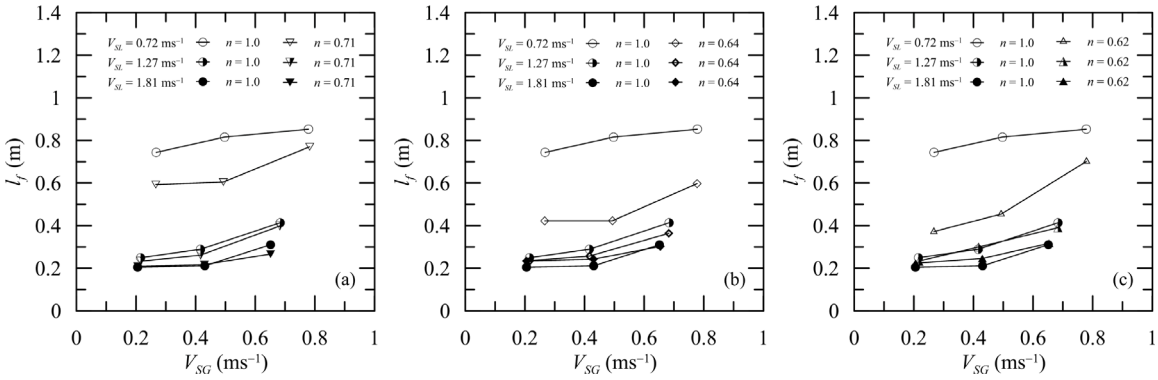

Fig. 13. Bubble length for all tested shear-thinning fluids.

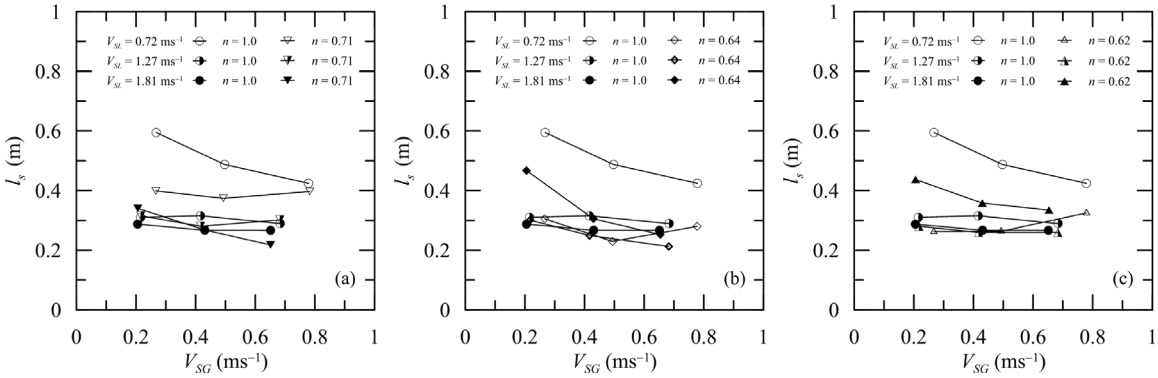

Fig. 14. Liquid slug length for all tested shear-thinning fluids.

A balance of forces yields the necessary diameter for bubbles not to migrate to the top region of the pipe and coalesce:

$$\tilde{d}_{\mathrm{cv}} \approx \left(\frac{6KV_m^n f_L^{n/2}}{2^{n/2}(\rho_L - \rho_G) g D^{n+1}} \right)^{\frac{1}{n+1}}. \tag{47}$$

According to Brauner (2001), the stable diameter for a dense dispersion is

$$\tilde{d}_{\max} = 2.22 C_H^{3/5} We_L^{-0.6} \left(\frac{\rho_m}{\rho_L(1-\alpha)} f_L \right)^{-0.4} \left(\frac{\alpha}{1-\alpha} \right)^{0.6}, \tag{48}$$

with $We_L = (\rho_L D V_m^2)/\sigma$, σ = surface tension.

Brauner (2001) makes clear that the value of C_H is not strict and can be tuned to better fit the available experimental data for some particular flow condition. A value of $C_H > 1$ represents a flow system where "not all the turbulent kinetic energy in the continuous phase is available for dispersing the other phase". Values of $C_H < 1$ should also not be completely ruled out. In the following, $C_H = 1$ is considered.

The stable α value can be found by making $\tilde{d}_{\mathrm{cv}} = \tilde{d}_{\max}$. A fitting to the experimental data shown in Fig. 25 suggested $\tilde{d}_{\mathrm{cv}}$ to be considered a function of n so that

$$8n^{1.5} \left(\frac{6KV_m^n f_L^{n/2}}{2^{n/2}(\rho_L - \rho_G) g D^{n+1}} \right)^{\frac{1}{n+1}} = 2.22 We_L^{-0.6} \left(\frac{\rho_m}{\rho_L(1-\alpha)} f_L \right)^{-0.4} \left(\frac{\alpha}{1-\alpha} \right)^{0.6}. \tag{49}$$

The term $8n^{1.5}$ in Eq. (49) is also not strict and can be fixed to better satisfy the data representing a specific fluid system. This particular formulation was found adequate to represent the high degree of aeration observed in the liquid slugs of the present experiments (Figs. 5 through 8). As previously mentioned, in the present

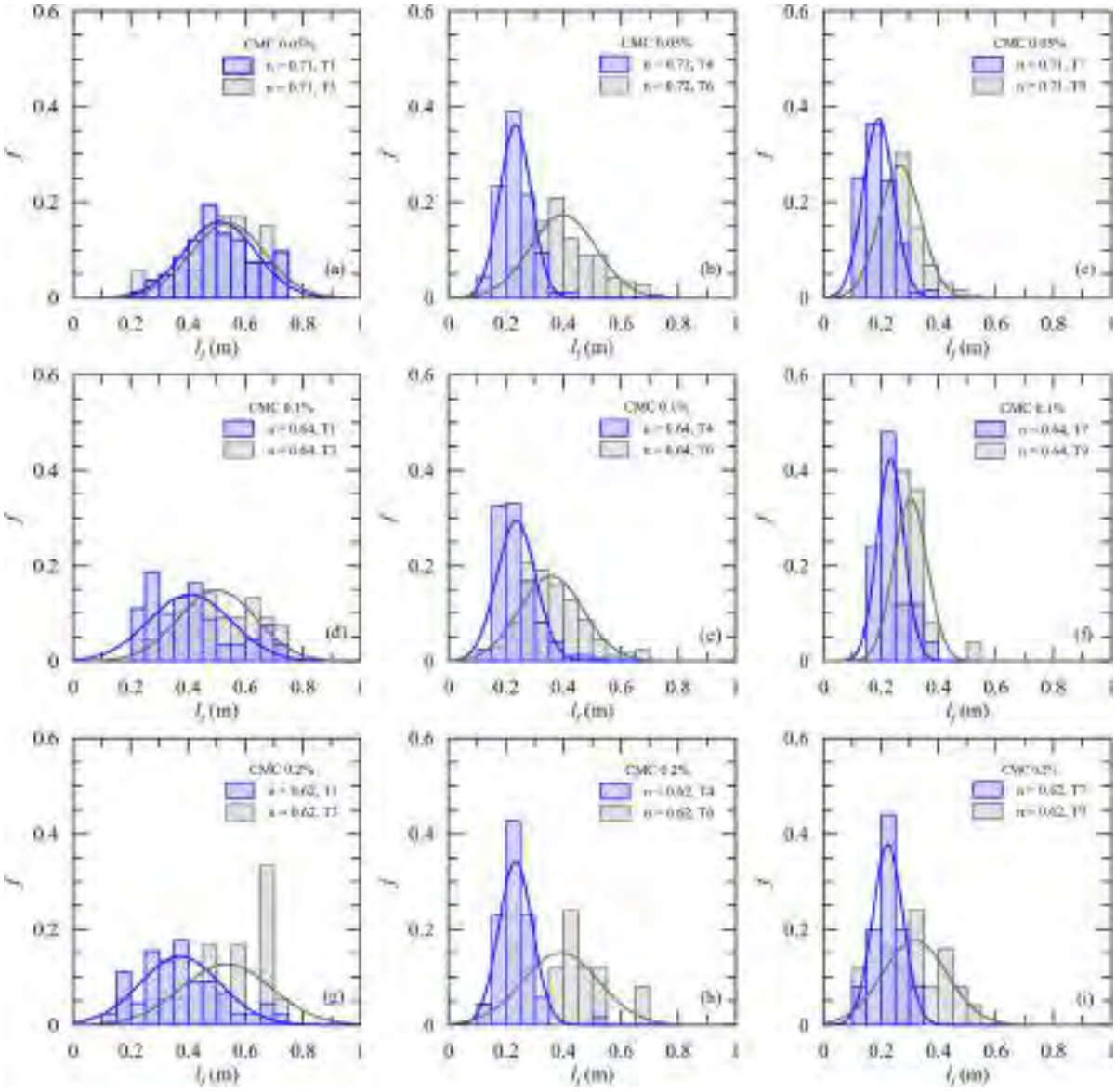

Fig. 15. Bubble length distributions for all tested shear-thinning fluids.

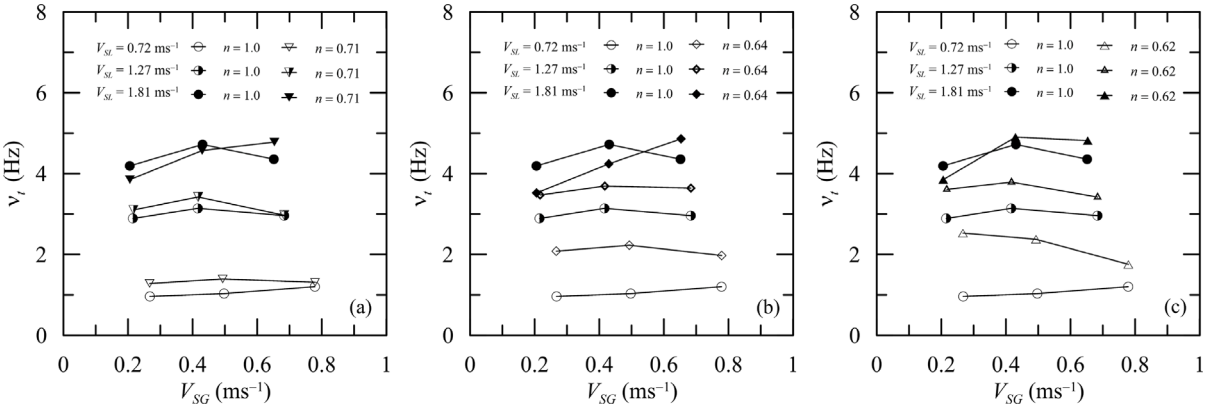

Fig. 16. Effect of flow rate and power-law index on slug frequency: comparison between air–water and (a) air-0.05% CMC solution, (b) air-0.1% CMC solution, (c) air-0.2% CMC solution.

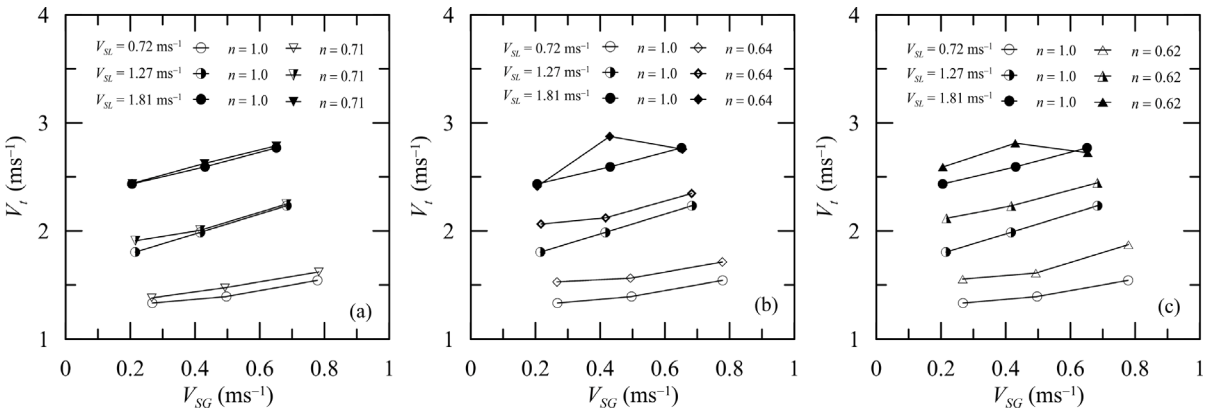

Fig. 17. Effect of flow rate and power-law index on the translational velocity of large bubbles.

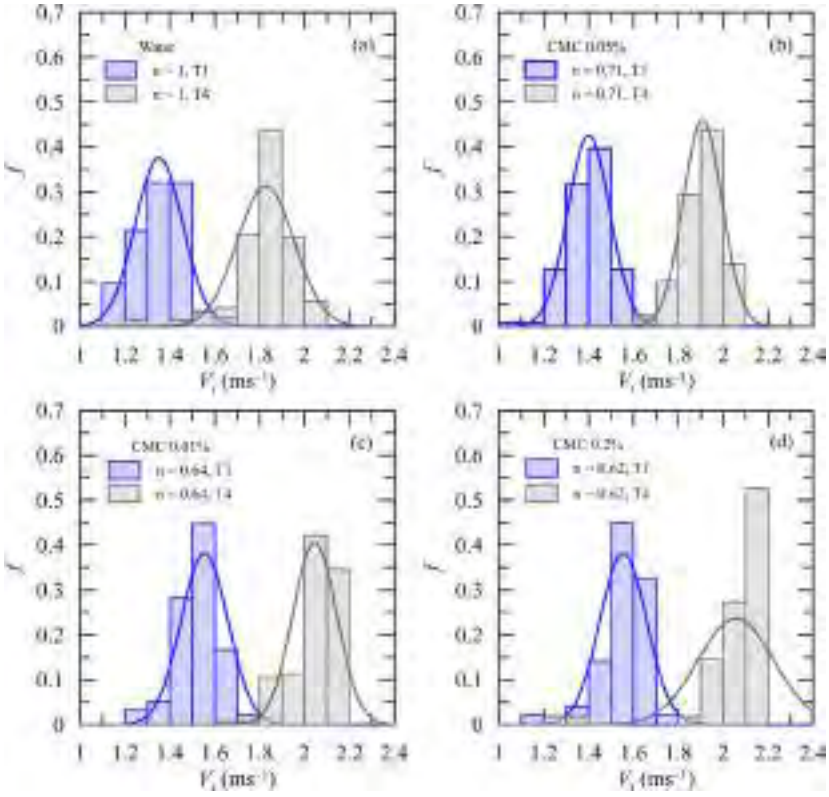

Fig. 18. Translational velocity distributions of large bubbles. T1: V_{SL} = 0.72 ms^{-1}, V_{SG} = 0.27 ms^{-1}; T4: V_{SL} = 1.27 ms^{-1}, V_{SG} = 0.22 ms^{-1}.

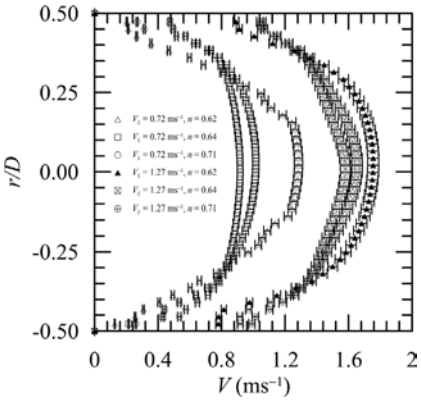

Fig. 19. Velocity field for single phase flows.

experiments gas was injected downstream of a 90° bend through an orthogonal orifice injector. This gas-injection condition was studied in Guerra et al. (2022) and was shown to induce the formation of a large number of small bubbles. Small bubbles are particularly difficult to coalesce in very viscous fluids (e.g., the air-CMC solutions of the present experiments), resulting in very aerated liquid slugs. The chosen power-law behavior is convenient to represent power-law fluids in view of the limiting condition that, as n tends to unity, Eq. (49) should reduce to the Newtonian case. The values in Eq. (49) were determined through a minimization process (linear regression) that considered the root-mean-square error (RMSE) of R_s. With the new expression, the RMSE of R_s is reduced to 11.4%.

We recall that water-CMC mixtures constitute a very popular mean to promote non-Newtonian power-law fluids in controlled laboratory experiments. The papers of Otten and Fayed (1976), Xu et al. (2009), Xu (2010), Jia et al. (2011) and Picchi et al. (2015) are all typical examples. As previously mentioned, the addition of low concentrations

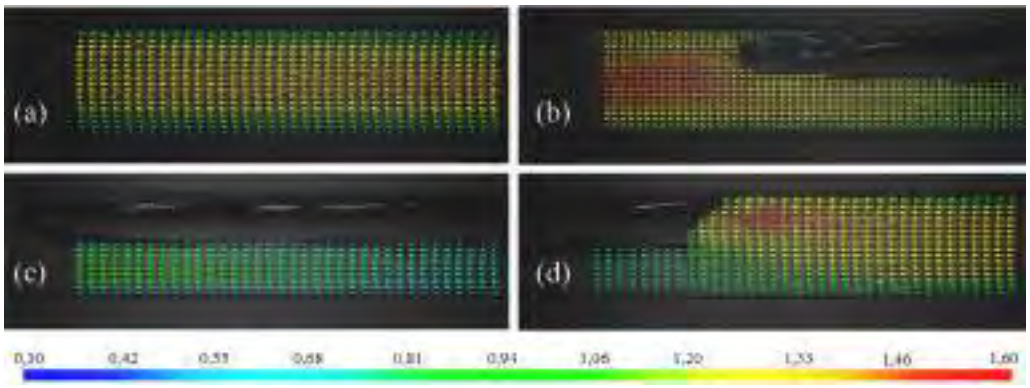

Fig. 20. Velocity field around a large bubble for CMC 0.1%, V_{SL} = 0.72 ms^{-1}, V_{SG} = 0.27 ms^{-1}. (a) Liquid slug, (b) nose, (c) main body, (d) tail.

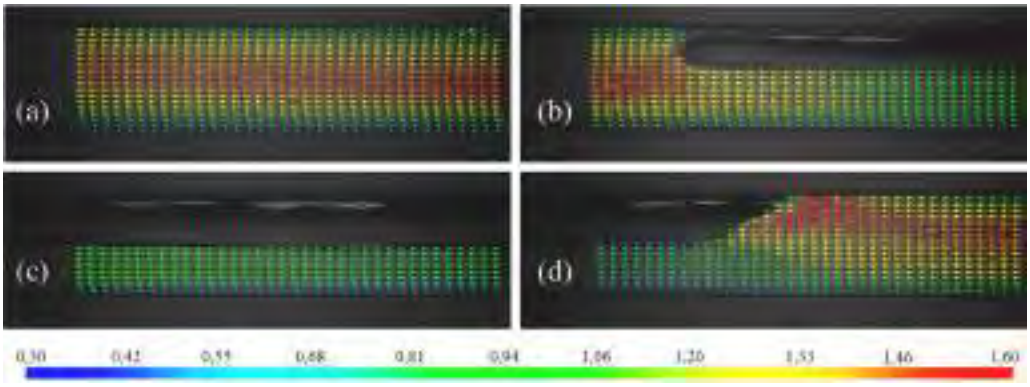

Fig. 21. Velocity field around a large bubble for CMC 0.2%, V_{SL} = 0.72 ms^{-1}, V_{SG} = 0.27 ms^{-1}. (a) Liquid slug, (b) nose, (c) main body, (d) tail.

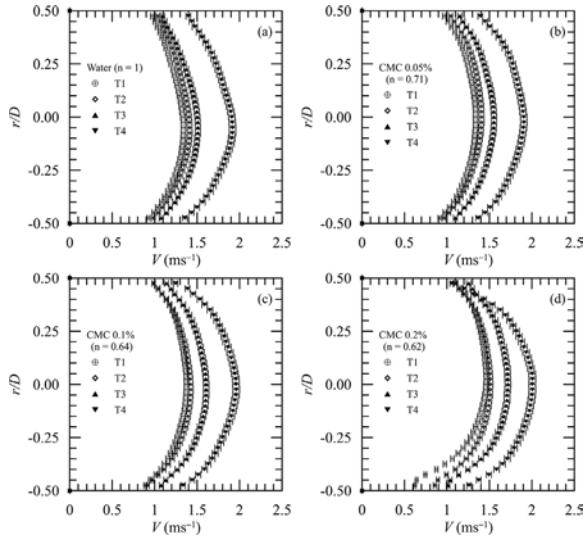

Fig. 22. Local velocity profiles in the liquid slug for water and CMC concentrations of (a) 0.0% (water only), (b) 0.05%, (c) 0.1% and (d) 0.2% (c). T1: V_{SL} = 0.72 ms^{-1}, V_{SG} = 0.27 ms^{-1}; T2: V_{SL} = 0.72 ms^{-1}, V_{SG} = 0.49 ms^{-1}; T3: V_{SL} = 0.72 ms^{-1}, V_{SG} = 0.78 ms^{-1}; T4: V_{SL} = 1.27 ms^{-1}, V_{SG} = 0.22 ms^{-1}.

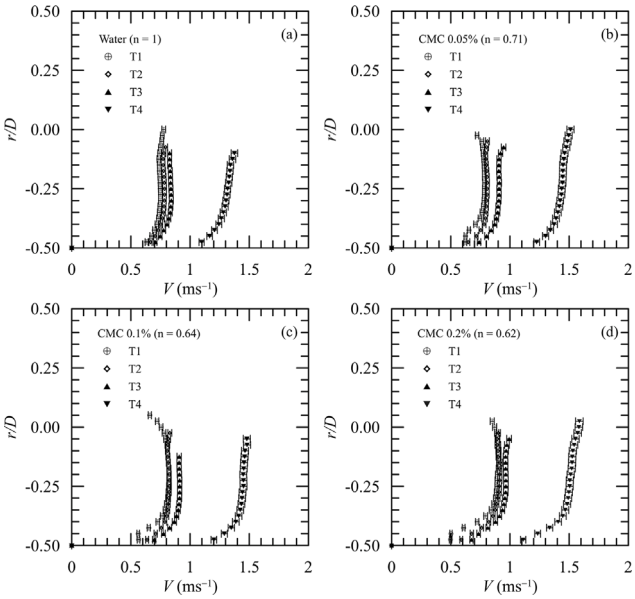

Fig. 23. Local velocity profiles in the films for water and CMC concentrations of (a) 0.0% (water only), (b) 0.05%, (c) 0.1% and (d) 0.2%. T1: V_{SL} = 0.72 ms^{-1}, V_{SG} = 0.27 ms^{-1}; T2: V_{SL} = 0.72 ms^{-1}, V_{SG} = 0.49 ms^{-1}; T3: V_{SL} = 0.72 ms^{-1}, V_{SG} = 0.78 ms^{-1}; T4: V_{SL} = 1.27 ms^{-1}, V_{SG} = 0.22 ms^{-1}.

of CMC to water produces a fluid that exhibits a high increase in viscosity with a shear-thinning behavior (Fig. 2), and a decrease in surface tension. The increase in viscosity is manifested through the proportionality consistency parameter (K), and the flow index (n). In the present experiments, values of K ranged between 0.023 and 0.157 (Pas^n) and values of n between 0.72 to 0.62 (Table 1). The changes in surface tension varied typically from 0.0667 Nm^{-1} (water) to 0.0525 Nm^{-1} (CMC mixtures), a maximum change of about 21%. This decrease in surface tension was observed not have any significant effect on the dynamics of bubble coalescence in the liquid slug. However, Figs. 5 to 8

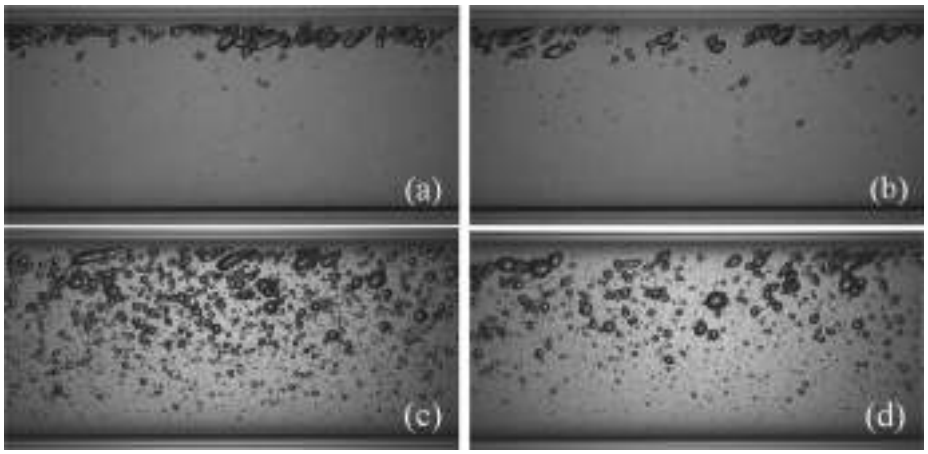

Fig. 24. Liquid slugs. V_{SL} = 1.27 ms^{-1}, V_{SG} = 0.68 ms^{-1}. (a, b) Water; (c, d) CMC 0.2%.

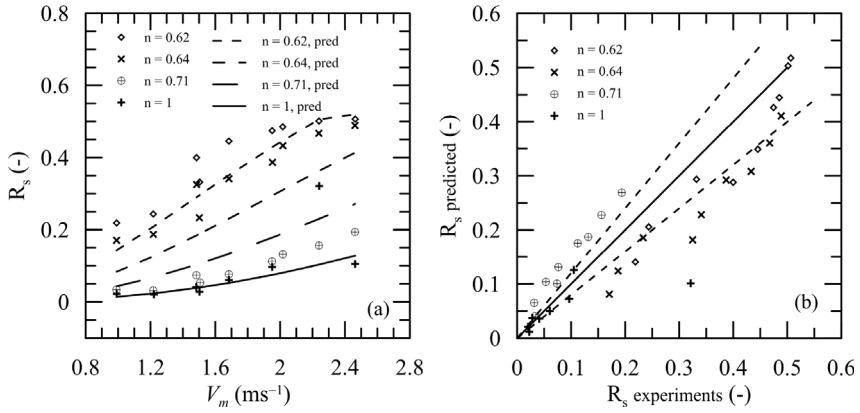

Fig. 25. Comparison of the predicted values of α (= 1 − R_s) with the present experimental data.

and Fig. 24 clearly show that the degree of aeration of the liquid slugs increases as the concentration of CMC in the mixture increases. It is also clear from these figures that the spatial distribution of small bubbles becomes more homogeneous as the concentration of CMC in the mixture increases. Please, note that the basis for comparison of Figs. 5 to 8 is the conservation of the superficial velocities of water and air.

The dynamics of small bubbles in the liquid slug region is described through Eqs. (45) to (49), where a balance between buoyant forces, viscous forces and turbulence is considered. The analysis considers the model of Brauner (2001) for prediction of the sizes of bubbles or drops in a turbulent flow field, which in turn is based on the Kolmogorov(1949)-Hinze(1955) theory for emulsification in turbulent flow. The model of Brauner (2001) considers changes in surface tension (Eq. (48), see the definition of We_L). The presently introduced theory (Eq. (49)) is thus capable of estimating the maximum size of bubbles considering the balance between the external forces that tend to deform the small bubbles and the counteracting surface tension forces. In the above developments, Eqs. (45) to (47) account for the increase in homogeneity in bubble distribution. Eq. (48) accounts for the stability of the dense dispersion in relation to coalescence processes.

Eq. (49) can be solved numerically to find α. This value is limited to 0.52. Results provided by Eq. (49) are also presented in Fig. 25.

5.2.2. ν_t behavior for a non-Newtonian liquid phase: analysis of existing correlations and a new formulation

An assessment of the existing models for the prediction of ν_t is shown in Table 4. In the present case, the correlations tended to largely under predict ν_t.

Table 4
Root-mean-square error of ν_t ($\sigma^n_{R_s}$) according to the various models and the present experimental data. *n* denotes Newtonian fluid; *nn* denotes non-Newtonian fluid.

Reference	$\sigma^n_{\nu_t}$ (%)	$\sigma^{nn}_{\nu_t}$ (%)
Gokcal et al. (2009)	94.8	79.5
Heywood and Richardson (1979)	44.8	44.1
Picchi et al. (2015)	47.6	66.1
Rosehart et al. (1975)	41.7	31.6
Schulkes (2011)	29.9	46.9
Gregory and Scott (1969)	43.5	43.5
Shell	27.3	40.9

The model of Gokcal et al. (2009) that was originally developed for highly viscous fluids (oil) under predicted ν_t by 94.8%. The best predictions for the air/water flows were provided by the Schulkes (2011) and Shell correlations with errors of 29.9 and 27.3% respectively. For the non-Newtonian solutions, the correlation of Rosehart et al. (1975) furnished the best results.

To propose a new correlation for ν_t that better represents the effects of fluid rheology, the method of Schulkes (2011) is applied.

An analysis of the present experimental data for the non-Newtonian fluids suggests

$$\Phi^{\text{mod}}(Re_{MR_{SL}}) = \begin{cases} \Phi(Re_{MR_{SL}}), & n > n_{\text{crit}}, \\ 6.94 Re^{-0.17}_{MR_{SL}}, & n \le n_{\text{crit}}, \end{cases} \tag{50}$$

where $Re_{MR_{SL}}$ is based on V_{SL} and n_{crit} is over 0.715. Here, we consider n_{crit} = 0.8.

Table 5
Model configurations for flow predictions according to the model of Dukler and Hubbard (1975).

Configuration	f	R_s	ν_t
0	Blasius	Andreussi et al. (1993)	Schulkes (2011)
1	Anbarlooei et al. (2015a)	Andreussi et al. (1993)	Schulkes (2011)
2	Blasius	Eq. (49)	Schulkes (2011)
3	Blasius	Andreussi et al. (1993)	Eq. (51)
4	Anbarlooei et al. (2015a)	Eq. (49)	Eq. (51)

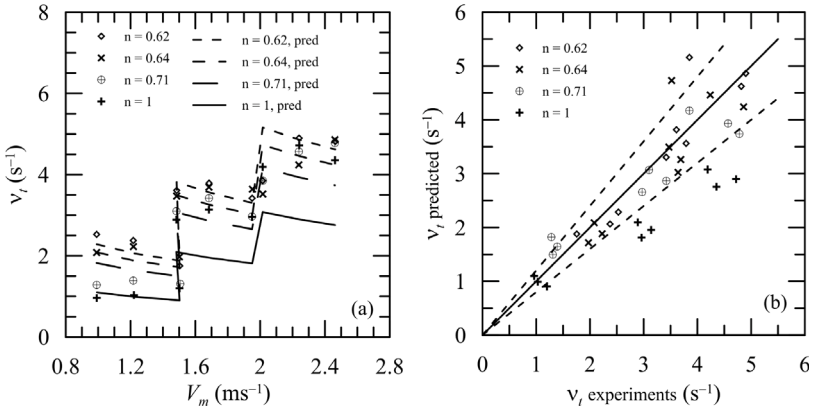

Fig. 26. Comparison of the predicted values of ν_t with the present experimental data.

The resulting expression for ν_t is

$$\nu_t = \Psi(R_s)\Phi^{\text{mod}}(Re_{M R_{SL}})\Theta(\beta, Fr_{SL})\frac{V_m}{D}. \tag{51}$$

Results furnished by Eq. (51) are displayed in Fig. 26.

5.3. Assessment of the theoretical models

The new proposed corrections for f_L, R_s and ν_t (Eqs. (41), (49), (51)) are tested next through the unit cell models of Dukler and Hubbard (1975) and Orell (2005). The model of Dukler and Hubbard (1975) is used to generate predictions of V_t and dP/dx. The formulation of Orell (2005) is used to predict dP/dx.

To isolate the different effects of the new proposed expressions, the model configuration shown in Table 5 is used. For the Orell (2005) model, the configurations are shown in Table 6.

The predictions of V_t through the model of Dukler and Hubbard (1975) with the present improvements is very good (Eqs. (41)–(49)–(51), Fig. 27). Predictions of V_t through the correlations of Bendiksen (1984), Petalas and Aziz (1998) and Smith et al. (2013) are also shown.

The root-mean-square error of V_t ($\sigma^{nn}_{V_t}$) for the predictions given by the theory of Dukler and Hubbard (1975) is 10.5%. The correlations of Bendiksen (1984) and Smith et al. (2013) give respectively $\sigma^{nn}_{V_t}$ = 9.7 and 10.9. The correlation of Petalas and Aziz (1998) furnishes $\sigma^{nn}_{V_t}$ = 19.0. The 10% error band on predictions of V_t for the non-Newtonian mixtures is of the order of the error band for predictions of water flow. This is an important result, which shows that the appropriate modeling of f_L, R_s and ν_t can generate good predictions of V_t through the theory of Dukler and Hubbard (1975).

Regarding the predictions of the pressure gradient, Fig. 28 shows distinctly that the isolate application of any of the proposed equations to the model of Dukler and Hubbard (1975) (Eqs. (41)–(49)–(51)) improves on the results of the standard formulation (Configuration 0). In particular, the application of all three combined equations (Configuration 4) gives the best agreement with the experimental data.

The modified model of Orell (2005) is analyzed in Fig. 29. The inclusion of the friction coefficient equation of Anbarlooei et al. (2015a) largely improves the predictions. As expected, the single consideration of Eq. (49) is not capable of furnishing better results than the standard formulation since the equation of Blasius plays a dominant role in the calculations. However, the combination of Eqs. (41) and (49) does not work well: data agreement is worsened.

Table 6
Model configurations for flow predictions according to the model of Orell (2005).

Configuration	f	R_s
0	Blasius	Andreussi et al. (1993)
1	Anbarlooei et al. (2015a)	Andreussi et al. (1993)
2	Blasius	Eq. (49)
3	Anbarlooei et al. (2015a)	Eq. (49)

Figs. 28 and 29 indicate that the specialized friction factor formulation of Anbarlooei et al. (2015a) results in better predictions of the flow properties through the models of Dukler and Hubbard (1975) and Orell (2005).

The model comparison shown in Figs. 28 and 29 depends strongly on Eq. (49), which was specially developed for flows with highly aerated liquid slugs. However, it would be of general interest to compare the present model with the data of other authors. An ample literature survey shows that the data of Xu et al. (2009) are well varied since they cover flows of fluids with five distinct rheological behavior. The data are also well reported, in particular, for two of the working fluids (air/CMC-3 and air/CMC-4).

A comparison of the presently introduced models with the data of Xu et al. (2009) is shown in Fig. 30. The tested models are Configurations 0 and 4 for the Dukler and Hubbard model (D&H0 and D&H4) and Configurations 0 and 3 for the Orell model (Or0 and Or3). For very small pressure drops when the flow conditions are very different, the predictions are poor. However, as dP/dx increases, the predictions become increasingly better. In fact, for dP/dx around 3 the experimental data furnish higher values of dP/dx compared to the theoretical predictions. Unfortunately, the paper of Xu et al. (2009) does not discuss the degree of aeration of the liquid slug (R_s) or shows a picture of this flow region. Hence, having any impression on the spatial configuration of the small bubbles, including their diameter distribution is not possible. The paper also lacks information on the frequency of passage of bubbles, ν_t. These two parameters are of fundamental importance as input data in the presently introduced models. This aspect severally hampers any attempt at further discussing the data

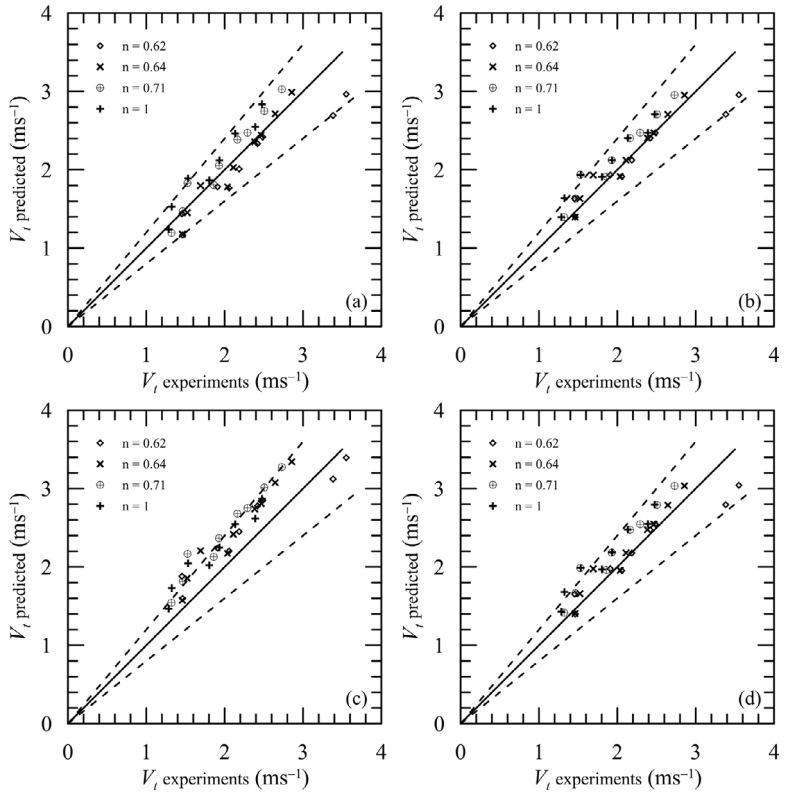

Fig. 27. Predictions of V_t through the model of Dukler and Hubbard (1975) with Configuration 4 (a). Other tested models: Bendiksen (1984) (b), Petalas and Aziz (1998) (c) and Smith et al. (2013) (d).

of Fig. 30. The overall agreement of the theory D&H4, however, is very satisfactory.

The model with the best performance was D&H4. To assess the several models, the conditions highlighted in Gonçalves et al. (2018) were strictly considered, that is, the mathematical and physical validity domains of unit-cell horizontal slug flow models. Model D&H4 was the model that most consistently provided converged solutions, with predictions 20% within the expected pressure drop values.

6. Final remarks

The present results have shown that the shear-thinning behavior of the liquid phase in slug flows has a substantial effect of the properties of the flow. In particular the work has shown that parameters f_L, R_s and v_t need an adequate modeling for the adequate description of pressure changes.

The shear-thinning behavior of the liquid phase together with the manner in which gas is injected into the flow (through a "T" connection) resulted in a very high aeration of the liquid slug, in much higher frequencies of bubble passage, much shorter bubble lengths and high pressure changes as compared to Newtonian liquid slug flows. Slug frequencies and pressure changes increased by as much as 250% and 125%, respectively. Two unit cell models were adapted through three new closure relations to represent the phenomenon. The predictions resulted in acceptable values of error.

CRediT authorship contribution statement

R. Baungartner: Investigation, Experimental measurements, Validation. **G.F.N. Gonçalves:** Investigation, Implementation of theoretical models, Validation. **J.B.R. Loureiro:** Methodology, Writing – review & editing, Project administration, Resources. **A.P. Silva Freire:** Conceptualization, Validation, Writing – original draft, Supervision.

Declaration of competing interest

The authors declare that they have no known competing financial interests or personal relationships that could have appeared to influence the work reported in this paper.

Data availability

Data will be made available on request

Acknowledgments

GFNG is thankful to CAPES for his research scholarship. APSF is grateful to the Brazilian National Research Council (CNPq) for the award of a Research Fellowship (No. 307232/2019-0). The work has been financially supported by FAPERJ through grant E-26/010.001275/2016 (Pronex Núcleo de Excelência em Turbulência).

References

Abdul-Majeed, G.H., 2000. Liquid slug holdup in horizontal and slightly inclined two-phase slug flow. J. Pet. Sci. Eng. 27 (1–2), 27–32.

Al-Safran, E., 2009. Investigation and prediction of slug frequency in gas/liquid horizontal pipe flow. J. Pet. Sci. Eng. 69, 143–155.

Al-Safran, E., Kora, C., Sarica, C., 2015. Prediction of slug liquid holdup in high viscosity liquid and gas two-phase flow in horizontal pipes. J. Pet. Sci. Eng. 133, 566–575.

Anbarlooei, H.R., Cruz, D.O.A., Ramos, F., Santos, C.M.M., Silva Freire, A.P., 2017a. On the connection between Kolmogorov microscales and friction in pipe flows of viscoplastic fluids. Physica D.

Anbarlooei, H.R., Cruz, D.O.A., Ramos, F., Silva Freire, A.P., 2015a. Phenomenological Blasius-type friction equation for turbulent power-law fluid flows. Phys. Rev. E 92 (6), 5–9.

Anbarlooei, H.R., Cruz, D.O.A., Ramos, F., Silva Freire, A.P., 2017b. Phenomenological friction equation for turbulent flow of Bingham fluids. Phys. Rev. E 96, 023107.

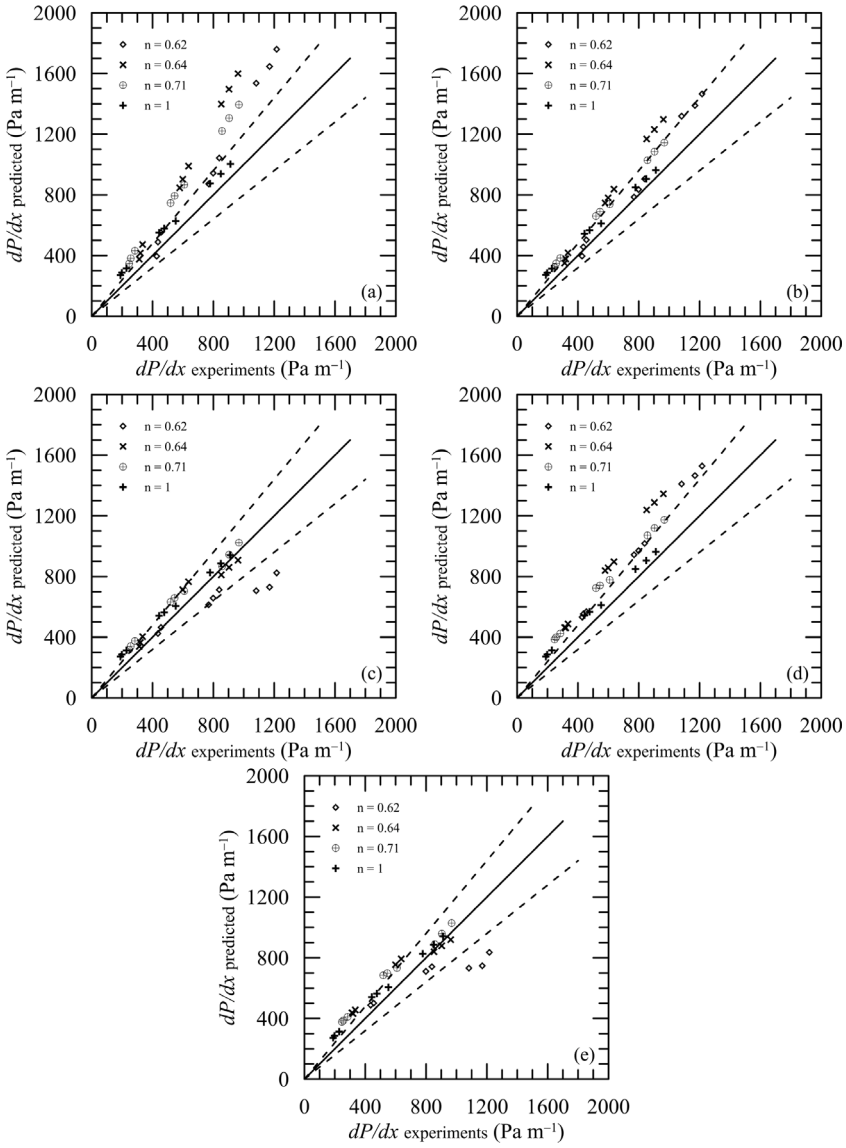

Fig. 28. Predictions of dP/dx through the model of Dukler and Hubbard (1975) and Configurations 0 (a) through 4 (e).

Anbarlooei, H.R., Cruz, D.O.A., Silva Freire, A.P., 2015b. A Blasius type friction equation for purely viscous non-Newtonian fluid. In: European Turbulence Conference. Euromech.

Andreussi, P., Bendiksen, K.H., Nydal, O.J., 1993. Void distribution in slug flow. Int. J. Multiph. Flow. 19 (5), 817–828.

Bandeira, F.J.S., Gonçalves, G.F.N., Loureiro, J.B.R., Silva Freire, A.P., 2017. Turbulence and bubble break up in slug flow with wall injection. Flow Turbul. Combust. 98, 923–945.

Barnea, D., Brauner, N., 1985. Holdup of the liquid slug in two phase intermittent flow. Int. J. Multiph. Flow. 1 (11), 43–49.

Benchabane, A., Bekkour, K., 2008. Rheological properties of carboxymethyl cellulose (CMC) solutions. Colloid Polym. Sci. 286 (10), 1173.

Bendiksen, K.H., 1984. An experimental investigation of the motion of long bubbles in inclined tubes. Int. J. Multiph. Flow. 10 (4), 467–483.

Brauner, N., 2001. The prediction of dispersed flow boundaries in liquid-liquid and gas-liquid systems. Int. J. Multiph. Flow. 27 (5), 885–910.

Celis, G., Rosero, C., Loureiro, J., Silva Freire, A.P., 2021. Breakup and coalescence of large and small bubbles in sudden expansions and contractions in vertical pipes. Int. J. Multiph. Flow. 137, 103548.

Chhabra, R.P., Richardson, J.F., 1984. Prediction of flow pattern for the co-current flow of gas and non-Newtonian liquid in horizontal pipes. Can. J. Chem. Eng. 62 (4), 449–454.

Dodge, D.W., Metzner, A.B., 1955. Turbulent flow of non-Newtonian systems. A.I.Ch.E. J. 5, 189–204.

Dukler, A.E., Hubbard, M.G., 1975. A model for gas-liquid slug flow in horizontal and near horizontal tubes. Ind. Eng. Chem. Fundam. 14 (4), 337–347.

Fagundes Netto, J.R., Gonçalves, G.F.N., Silva Freire, A.P., 2019. Statistical Moments Transport Model for the prediction of slug flow properties. Int. J. Multiph. Flow. 120, 103086.

Gokcal, B., Al-Sarkhi, A., Sarica, C., Al-Safran, E., 2009. Prediction of slug frequency for high viscosity oils in horizontal pipes. In: SPE Annual Technical Conference and Exhibition. pp. 1–13.

Gonçalves, G.F.N., Baungartner, R., Loureiro, J.B.R., Silva Freire, A.P., 2018. Slug flow models: Feasible domain and sensitivity to input distributions. J. Petrol. Sci. Eng. 169, 705–724.

Gregory, G.A., Nicholson, M.K., Aziz, K., 1978. Correlation of the liquid volume fraction in the slug for horizontal gas-liquid slug flow. Int. J. Multiph. Flow. 4 (1), 33–39.

Gregory, G.A., Scott, D.S., 1969. Correlation of liquid slug velocity and frequency in horizontal cocurrent gas-liquid slug flow. AIChE J. 15, 933–935.

Guerra, L.A.O., Temer, B.O., Loureiro, J.B.R., Freire, A.P.S., 2022. Experimental study of gas-lift systems with inclined gas jets. J. Petrol. Sci. Eng. 216, 110749.

Heywood, N.I., Richardson, J.F., 1979. Slug flow of air/water mixtures in a horizontal pipe: Determination of liquid holdup by γ-ray absorption. Chem. Eng. Sci. 34, 17–30.

JCGM, 2010. Evaluation of measurement data - Guide to the expression of uncertainty in measurement. JCGM 2010 100, 134.

Jia, N., Gourma, M., Thompson, C.P., 2011. Non-Newtonian multi-phase flows: On drag reduction, pressure drop and liquid wall friction factor. Chem. Eng. Sci. 66 (20), 4742–4756.

Kora, C., Sarica, C., Zhang, H.-Q., Al-Sarkhi, A., Fahd, K., Alsafran, E.M., 2011. Effects of high oil viscosity on slug liquid holdup in horizontal pipes. In: SPE the Canadian Unconvetional Resources Conference, 2011. pp. 1–15.

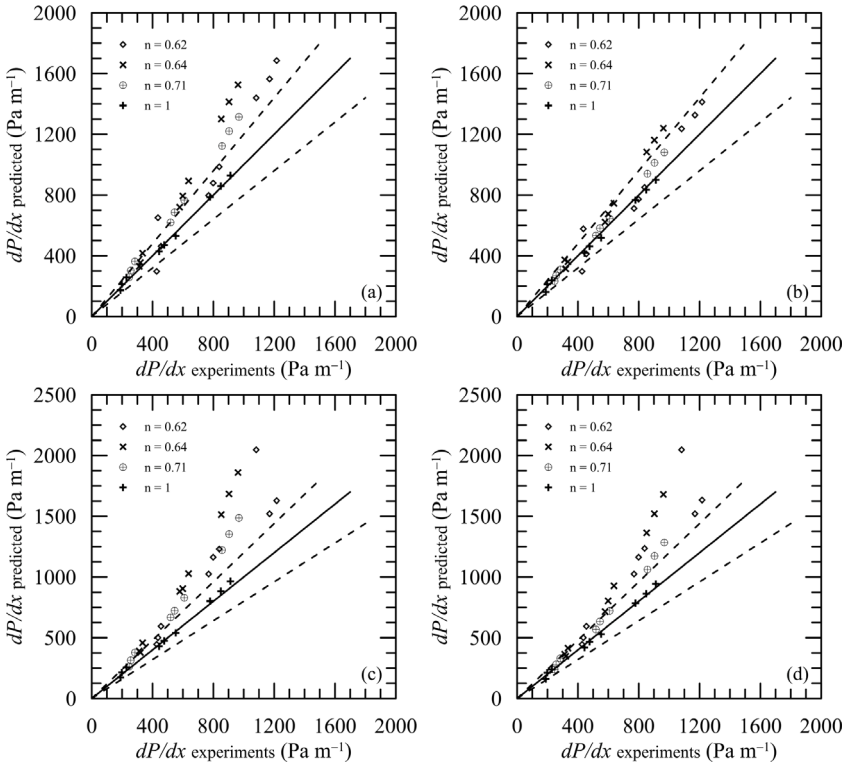

Fig. 29. Predictions of dP/dx through the model of Orell (2005) and Configurations 0 (a) through 3 (d).

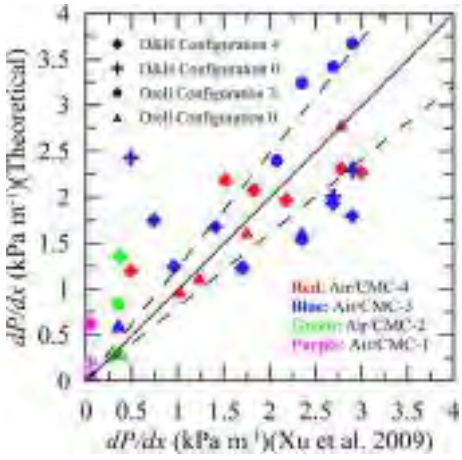

Fig. 30. Comparison between the present theory and the pressure data of Xu et al. (2009).

Loureiro, J.B.R., Silva Freire, A.P., 2013. Asymptotic analysis of turbulent boundary-layer flow of purely viscous non-Newtonian fluids. J. Non-Newton. Fluid Mech. 199, 20–28.

Ma, Y.P., Chung, N.M., Pei, B.S., Lin, W.K., Hsu, Y.Y., 1991. Two simplified methods to determine void fractions for two-phase flow. Nucl. Technol. 94 (1), 124–133.

Magalhaes, G.R., Gonçalves, G.F.N., Loureiro, J.B.R., Silva Freire, A.P., 2013. An experimental investigation of the effects of gas solubility on the properties of horizontal slug flow. Int. J. Multiph. Flow. 50, 33–40.

Matamoros, L.M.C., Loureiro, J.B.R., Silva Freire, A.P., 2014. Length-area-volume of long bubbles in horizontal slug flow. Int. J. Multiph. Flow. 65, 24–30.

Metzner, A.B., Reed, J., 1955. Flow of non-Newtonian fluids – Correlation of the laminar, transition and turbulent-flow regions. A.I.Ch.E. J. 1, 434–440.

Nicklin, D.J., Wilkes, J.O., Davidson, J.F., 1962. Two-phase flow in vertical tubes. Trans. Inst. Chem. Eng. 40, 61–68.

Oliver, D.R., Hoon, A.Y., 1968. Two-phase non-Newtonian Flow. Part I: Pressure drop and hold-up. Chem. Eng. Res. Des. 46.

Orell, A., 2005. Experimental validation of a simple model for gas liquid slug flow in horizontal pipes. Chem. Eng. Sci. 60 (5), 1371–1381.

Otten, L., Fayed, A.S., 1976. Pressure drop and drag reduction in two-phase non-Newtonian slug flow. Can. J. Chem. Eng. 54 (1–2), 111–114.

Petalas, N., Aziz, K., 1998. A mechanistic model for multiphase flow in pipes. In: 49th Annual Technical Meeting of Petroleum Society of the Canadian Institute of Mining, Metallurgy & Petroleum. Petroleum Society of Canada.

Picchi, D., Manerba, Y., Correra, S., Margarone, M., Poesio, P., 2015. Gas/shear-thinning liquid flows through pipes: Modeling and experiments. Int. J. Multiph. Flow. 73, 217–226.

Rosehart, R.G., Rhodes, E., Scott, D.S., 1975. Studies of gas-liquid (non-Newtonian) slug flow: Void fraction meter, void fraction and slug characteristics. Chem. Eng. J. 10 (1), 57–64.

Rosero, C.M.P., Celis, C.E.O., Loureiro, J.B.R., Freire, A.P.S., 2022. Phenomenology of bubble breakup and coalescence in sudden expansions and contractions in vertical pipes. Int. J. Multiph. Flow. 146, 103840.

Schulkes, R., 2011. Slug Frequencies Revisited. In: 15th International Conference on Multiphase Production Technology, no. 1969. pp. 311–325.

Smith, I.E., Nossen, J., Unander, T.E., 2013. Improved holdup and pressure drop predictions for multiphase flow with gas and high viscosity oil. In: 16th International Conference on Multiphase Production Technology.

Taitel, Y., Barnea, D., 1990. A consistent approach for calculating pressure drop in inclined slug flow. Chem. Eng. Sci. 45 (5), 1199–1206.

Ujang, P.M., Lawrence, C.J., Hale, C.P., Hewitt, G.F., 2006. Slug initiation and evolution in two-phase horizontal flow. Int. J. Multiph. Flow. 32 (5), 527–552.

Wang, Y.P., Pei, B.S., Lin, W.K., 1991. Verification of using a single void fraction sensor to identify two-phase flow patterns. Nucl. Technol. 95 (1), 87–94.

Xu, J.-Y., 2010. Investigation on average void fraction for air/non-Newtonian power-law fluids two-phase flow in downward inclined pipes. Exp. Therm Fluid Sci. 34 (8), 1484–1487.

Xu, J.-Y., 2013. A simple correlation for prediction of the liquid slug holdup in gas/non-Newtonian fluids: Horizontal to upward inclined flow. Exp. Therm Fluid Sci. 44, 893–896.

Xu, J.-Y., Wu, Y.-Y., Li, H., Guo, J., Chang, Y., 2009. Study of drag reduction by gas injection for power-law fluid flow in horizontal stratified and slug flow regimes. Chem. Eng. J. 147 (2–3), 235–244.